From observed transitions to hidden paths in Markov networks

Alexander M. Maier [1], Udo Seifert [1], and Jann van der Meer [1,2]
[1]II. Institut für Theoretische Physik, Universität Stuttgart, 70550 Stuttgart, Germany
[2]Department of Physics No. 1, Graduate School of Science, Kyoto University, Kyoto 606-8502, Japan

(Received 16 April 2025; accepted 24 June 2025; published 17 July 2025)

The number of observable degrees of freedom is typically limited in experiments. Here we consider discrete Markov networks in which an observer has access to a few visible transitions and the waiting times between these transitions. Focusing on the underlying structure of a discrete network, we present methods to infer local and global properties of the network from observed data. First, we derive bounds on the microscopic entropy production along the hidden paths between two visible transitions, which complement extant bounds on mean entropy production and affinities of hidden cycles. Second, we demonstrate how the operationally accessible data encodes information about the topology of shortest hidden paths, which can be used to identify potential clusters of states or exclude their existence. Finally, we outline a systematic way to combine the inferred data, resulting in an algorithm that finds the candidates for a minimal graph of the underlying network, i.e., a graph that is part of the original one and compatible with the observations. Our results highlight the interplay between thermodynamic methods, waiting-time distributions, and topological aspects like network structure, which can be expected to provide novel insights in other setups of coarse graining as well.

DOI: 10.1103/p4k1-1dvb

I. INTRODUCTION

On the microscopic scale, the laws of thermodynamics acquire a form that is different to the expressions commonly used for macroscopic descriptions. As thermal noise significantly affects the trajectory of a given physical system embedded in a thermal environment, we have to resort to a stochastic rather than deterministic description of the dynamics. The framework of stochastic thermodynamics adopts this conceptual shift for thermodynamic quantities such as entropy production, work, and heat, which are now understood as trajectory-dependent random variables [1–5]. As a result, the thermodynamic properties of a physical system are now closely related to its stochastic dynamics, so that, given the right tools, we are able not only to incorporate the thermodynamic laws into a physical model but also to investigate the reverse problem, namely, the inference of dynamical aspects of a given physical system from its thermodynamic characteristics.

Such questions are studied in the emerging field of thermodynamic inference [6], which focuses on physical systems that can be observed only partially. In such a situation, the principles of stochastic thermodynamics cannot be applied directly, and the development of appropriate tools for inference constitutes one of the main tasks of this applied branch of stochastic thermodynamics. Much of the recent research in this field can be roughly sorted into one of two categories. A substantial number of studies focus on a specific nonequilibrium phenomenon and quantify the amount of dissipation implied by such an observation. Typically formulated as a lower bound on a quantifier for nonequilibrium like entropy production, such results include, e.g., the preeminent thermodynamic uncertainty relation [7–9], speed limits and transport results [10–14], response inequalities [15–17], bounds on the coherence of oscillations [18,19], and bounds in terms of correlation or waiting times [20–22].

This first category of results is complemented by a second one that places more emphasis on how the coarse-grained dynamics, i.e., the dynamics at the observable level, relates to the thermodynamics on the microscopic level. A rough classification of studies in this direction can be made by distinguishing the assumed observables and the mathematical structure of the coarse-grained process. Older works mainly focus on state lumping or decimation techniques, which result in phenomenological equations for the dynamics [6,23,24]. Over time, attention gradually shifted from the states to the currents along observed edges connecting them [25–27], a development that culminated in a thermodynamically consistent framework for coarse graining based on the transitions themselves [28,29]. One reason for this shift is that more powerful technical tools can be employed to connect dynamics and thermodynamics. Whereas in the case of state lumping typically only lower bounds on the mean entropy production rate expressed as a Kullback-Leibler divergence are possible [30–32], the more recent transition-based description allows for stronger results on the trajectory level, which include fluctuation relations [28,33] and a meaningful identification of a coarse-grained entropy production [34,35] even in the presence of time-dependent driving. Conceptually, these methods are able to include waiting times in their framework, a trait

Published by the American Physical Society under the terms of the Creative Commons Attribution 4.0 International license. Further distribution of this work must maintain attribution to the author(s) and the published article's title, journal citation, and DOI.

that is shared by related coarse-graining schemes that rely on milestoning [36,37], Markovian events [34,35,38], and trimming [39]. Apart from studying specific nonequilibrium phenomena or coarse-grained models, we might speculate about a third direction of inference that attempts to uncover not only thermodynamic but also dynamical or topological features of the underlying microscopic model. In this work, we assume that the underlying dynamics takes place in a discrete, finite configuration space and is described by a master equation, which is a common assumption within stochastic thermodynamics. We study the scenario that an external observer can register transitions between some pairs of states, whereas the states themselves and the remaining transitions remain inaccessible. In this setting, which is further detailed in Sec. II, we propose a number of novel approaches that reveal local and global properties of the underlying microscopic model, thereby extending the transition-based methods introduced in Refs. [28,29].

A common theme in the methods introduced in this work is the focus on microscopic paths, i.e., the possible trajectories in the hidden part of the system that take place between two observed transitions. One of our main results is a constructive statement regarding the existence of microscopic paths between particular transitions whose entropy production is larger or smaller than a particular, operationally determinable threshold. We provide the precise formulation of this statement and a numerical demonstration in Sec. III. The remainder of our results is built around a systematic connection between distributions of the waiting time between successive transitions and the minimal number of hidden transitions that take place in between, which is detailed in Sec. IV. Although this technique itself is not new (see, e.g., Refs. [28,40] for states and transitions, respectively), we present two novel refinements that focus on structural properties of the network on which the dynamics takes place. First, such structural information may provide insights into whether a network contains distinct clusters, a hypothesis that will be formulated more rigorously in Sec. V. Second, we may speculate about whether a systematic way of combining the inferable topological information is sufficient to reconstruct the entire microscopic model or a minimal variant of it. Our proposal towards this challenging goal is presented as an algorithm in Sec. VI. We discuss our methods and their limitations in Sec. VII before concluding with an outlook on potential future work in Sec. VIII.

II. SETUP

We consider a connected network of N states $i \in \{1, 2, \dots, N\}$. The state $i(t)$ of the system at time t follows a stochastic dynamics with instantaneous transitions between states that share an edge in the underlying graph. Transitions from state i to j occur according to a time-independent rate k_{ij}, which fulfills the local detailed balance condition $k_{ij}/k_{ji} = \exp(F_i - F_j + f_{ij})$ with free energy F_i of state i and non-conservative contribution $f_{ij} = -f_{ji}$ in units of thermal energy. Hence, in the graph, edges come in pairs, which we will call links. Moreover, the rates k_{ij} generate the dynamics of the occupation probability $p_i(t)$ of state i at time t, which obeys the master equation

$$\partial_t p_i(t) = \sum_j [p_j(t)k_{ji} - p_i(t)k_{ij}]. \tag{1}$$

In the long-time limit $t \to \infty$, $p_i(t)$ reaches a stationary state p_i^{s} with constant net current $j_{ij}^{\mathrm{s}} = p_i^{\mathrm{s}}k_{ij} - p_j^{\mathrm{s}}k_{ji}$ through the link from i to j. We assume that the network has reached this steady state throughout the paper.

We assume an observer for whom the underlying Markovian dynamics of the network is only partially accessible. In particular, the observer can register passages along m pairs of edges and can distinguish forward from backward transitions. In the steady state, the rate of observed transitions $I = (ij)$ is given by $P(I) \equiv p_i^{\mathrm{s}}k_{ij}$. The remaining transitions and the states of the network are hidden from the observer, as illustrated in Fig. 1(a) for the case $m = 1$. With access to a few transitions only, the observer aims at learning about the topology and the kinetics of the partially hidden network from measured data.

These data characterize the registered effective dynamics through waiting-time distributions of the form [28,29]

$$\Psi_{I\to J}(t) \equiv P(J, t|I, t_0 = 0) = k_{kl}p_k(t|j, 0), \tag{2}$$

where $I = (ij)$, $J = (kl)$ and t is the time since registering transition I. The function $\Psi_{I\to J}(t)$ characterizes the probability distribution of registering transition J after waiting time t given that I was observed at $t_0 = 0$. Its normalization is $\sum_J \int_0^\infty \Psi_{I\to J}(t)\mathrm{d}t = 1$. Since the underlying state of the network immediately before a transition is unique, the Markov property of the underlying dynamics ensures that the statistics entering $\Psi_{I\to J}(t)$ does not depend on the past prior to I.

Next, using the reverse transitions $\tilde{I} = (ji)$, $\tilde{J} = (lk)$ of I and J, we define

$$\hat{a}_{IJ}(t) \equiv \ln\frac{P(I)}{P(J)} + \ln\frac{\Psi_{I\to J}(t)}{\Psi_{\tilde{J}\to\tilde{I}}(t)}. \tag{3}$$

This quantity is time-independent when there is only one self-avoiding path between the two visible transitions, such as in a unicyclic network with one visible link. This time independence of $\hat{a}_{IJ}(t)$ is a manifestation of a more general symmetry in waiting-time distributions between forward and backward paths that holds true as long as there are no corresponding underlying paths that include a part of a cycle with nonzero affinity [28,34,41,42]. The same quantity also qualifies for an interpretation as an expression for entropy production that fluctuates on the coarse-grained level [34,35].

In addition to the operation $\tilde{\cdot}$, which yields the reverse transition of a given transition, we introduce the signs $+$ and $-$ as subscripts to label transitions for later convenience. These subscripts allow us to concisely specify links as a pair of edges, as in, e.g., $I_\pm$. Changing the sign in the subscript thus has the same effect as applying the tilde operation, since the edge I_+ is the reverse of I_- and vice versa.

III. BOUND ON ENTROPY PRODUCTION OF MICROSCOPIC PATHS

Our first result combines thermodynamic and topological reasoning to conclude the existence of particular microscopic

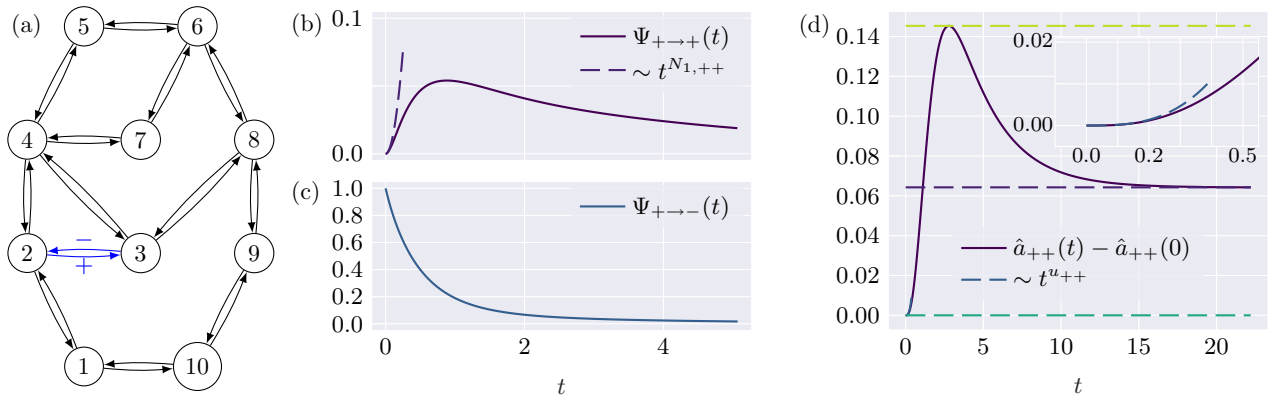


FIG. 1. Waiting-time distributions in a multicyclic Markov network. (a) Graph of a network, with transition rates given in Appendix D 1. Blue edges $\pm$ are visible while other edges and states are hidden. (b) Waiting-time distribution $\Psi_{+\to+}(t)$ for two consecutive $+$ transitions. The distribution is proportional to $t^{N_{1,++}}$ in the short-time limit, which yields the number $N_{1,++} = 2$ of hidden transitions along the shortest cycle containing $\pm$. (c) Waiting-time distribution $\Psi_{+\to-}(t)$ of the observed sequence $+ \to -$. The value $\Psi_{+\to-}(0)$ yields the rate of the transition $-$. (d) The difference $\hat{a}_{++}(t) - \hat{a}_{++}(0)$, which enters u_{++} in Eq. (13). Its short-time limit is proportional to $t^{u_{++}}$ with $u_{++} = N_{2,++} - N_{1,++} = 3$. The horizontal dashed lines mark local extrema of $\hat{a}_{++}(t) - \hat{a}_{++}(0)$. The global extrema yield bounds on cycle affinities as we will discuss in Sec. III.

paths (without self-crossings) whose entropy production exceeds or falls below a certain threshold. It is worth noting that the bound involves the entropy production of an individual microscopic path rather than the average dissipation of a class of paths or trajectories that become indistinguishable after coarse graining. We limit this section to the presentation, discussion, and illustration of the result and refer to Appendix A for the proof.

A. Result and discussion

It is sensible to speculate whether we can attribute thermodynamic meaning to the ratio of waiting-time distributions defined in Eq. (3). Here we present an interpretation of the quantity $\hat{a}_{IJ}(t)$ as a bound on the extremal microscopic entropy production along direct paths γ connecting the transition I to J. As discussed in more detail below, this perspective complements extant relations establishing $\hat{a}_{IJ}(t)$ as a lower bound on the average dissipation of all paths from I to J [34] and as an estimator for cycle affinities in the case $I = J$ [28].

The novel bound introduced in this work relates the extremal values of $\hat{a}_{IJ}(t)$ as a function of t to the microscopic entropy production $\Delta s[\hat{\gamma}]$ of particular cycle-free paths $\hat{\gamma}$. By removing all closed loops from a given microscopic path γ, we obtain an associated cycle-free path $\hat{\gamma}$ that we call the trimmed path. As an example, for the network depicted in Fig. 2 and the transitions $I = 7 \to 4$ and $J = 9 \to 10$, a possible microscopic path γ and its corresponding trimmed counterpart $\hat{\gamma}$ read

$$\begin{aligned} \gamma &= \xrightarrow{I} 4 \to 3 \to 2 \to 4 \to 3 \to 8 \to 6 \to 8 \to 9 \xrightarrow{J} \text{ and} \\ \hat{\gamma} &= \xrightarrow{I} 4 \qquad\qquad\quad \to 3 \to 8 \qquad\qquad\quad \to 9 \xrightarrow{J}, \end{aligned} \tag{4}$$

respectively.

We can now formulate the main result of this section,

$$\min_{\hat{\gamma}|I\to J} \Delta s[\hat{\gamma}] \leqslant \inf_t \hat{a}_{IJ}(t) \leqslant \sup_t \hat{a}_{IJ}(t) \leqslant \max_{\hat{\gamma}|I\to J} \Delta s[\hat{\gamma}], \tag{5}$$

which is proved in Appendix A and bounds the extremal values of the microscopic entropy production $\Delta s[\hat{\gamma}]$ that are possible for trimmed paths. The maximum and minimum are taken over all possible trimmed paths $\hat{\gamma}$ that start with the transition I, end with the transition J, and do not contain any other observed transitions. The term $\Delta s[\hat{\gamma}]$ includes the contribution to entropy production due to the initial jump I but excludes the last jump J. We note that there are only finitely many distinct cycle-free paths $\hat{\gamma}$, so that the maximal and minimal values of $\Delta s[\hat{\gamma}]$ are finite. In particular, the bound remains meaningful in the presence of hidden cycles, whereas quantities like $\max_\gamma \Delta s[\gamma]$ typically diverge in such cases.

Since each trimmed path $\hat{\gamma}$ corresponds to a topologically distinct pathway from I to J, so that the inequalities (5) combine topological and thermodynamic aspects in a similar way as bounds on cycle affinities do, to which they reduce when specifying $I = J$. These aspects are made even more explicit when reformulating the result (5) as a statement about the existence of particular microscopic paths in the hidden network. First, a microscopic path γ_+ from I to J that does not contain any loops or other observed transitions must exist and satisfies the condition

$$\Delta s[\gamma_+] \geqslant \sup_t \hat{a}_{IJ}(t). \tag{6}$$

In other words, not only are there microscopic paths whose entropy production exceeds the value $\sup_t \hat{a}_{IJ}(t)$, but such paths can even be found without completing any hidden cycles. A similar existence statement can be made for a path γ_- from I to J, which satisfies

$$\Delta s[\gamma_-] \leqslant \inf_t \hat{a}_{IJ}(t) \tag{7}$$

and again contains neither loops nor any other visible transitions apart from I and J.

Before providing an illustration for these results, we briefly discuss their relation to similar-looking bounds published earlier. First, Ref. [34] interprets the same quantity $\hat{a}_{IJ}(t)$ as a coarse-grained entropy production $\Delta S_{I\to J}(t)$, which

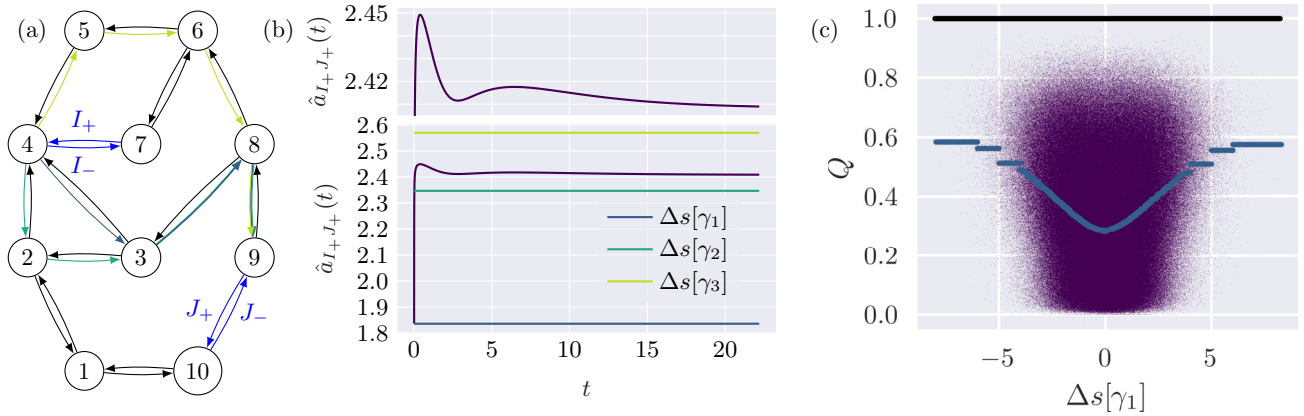


FIG. 2. Entropy production along paths in a multicyclic 10-state Markov network. (a) Graph with highlighted paths between visible transitions of the network with transition rates given in Appendix D 2. Only transitions $I_\pm, J_\pm$ along the blue edges are visible, whereas states and the remaining transitions are hidden. Three different possible paths between states 4 and 9, i.e., between the transitions I_+ to J_+ are highlighted: The shortest connection along $(4389) = 4 \to 3 \to 8 \to 9$ is marked in blue, whereas the paths (42389) and (45689) are highlighted in teal and olive green, respectively. In this order, these paths that connect I_+ to J_+ define γ_1, γ_2, and γ_3. (b) Time dependence of $\hat{a}_{I_+J_+}(t)$ as the waiting time t between the initial transition I_+ and the final transition J_+ is varied (purple curve) compared to the entropy production Δs of three different possible microscopic paths from I_+ to J_+ (horizontal lines). Except for paths containing closed loops, these three paths are the only possible ones from I_+ to J_+. Therefore, the result (5) implies that $\hat{a}_{I_+J_+}(t)$ stays bounded between the highest and lowest horizontal line for all t. In the figure, the value of the lower bound is attained in the limit $t \to 0$, because $\lim_{t\to 0} \hat{a}_{I_+J_+}(t)$ precisely recovers the entropy production of the path with the lowest number of intermediate states if this path is unique. (c) Illustration of the quality of the bound (5). We depict the quality factor $Q = \sup_t |\hat{a}_{I_+J_+}(t) - \Delta s[\gamma_1]| / \max_{i\in\{1,2,3\}} |\Delta s[\gamma_i] - \Delta s[\gamma_1]|$ for the estimator $\max_t |\hat{a}_{I_+J_+}(t) - \Delta s[\gamma_1]|$, which satisfies $0 \leqslant Q \leqslant 1$ by virtue of Eq. (5), as indicated by the horizontal line. The value Q is calculated for 1 731 699 randomly selected configurations of transition rates, more details are given in Appendix D 2 (purple dots). The average performance of the quality factor ranges from $Q \simeq 0.3$ to $Q \simeq 0.6$ and is measured as a binned mean grouping similar values of $\Delta s[\gamma_1]$ (blue lines).

satisfies an inequality of the form $\Delta S_{I\to J}(t) \leqslant \langle \Delta s[\gamma] | I \xrightarrow{t} J \rangle$ for each value of t, where the average is taken over all microscopic paths γ that are consistent with the coarse-grained data, i.e., all paths γ in the hidden network that start with a transition I followed by a transition J after time t. Second, the sequence of inequalities (5) is stronger than a conceptually related bound on affinities of hidden cycles also published in Ref. [34], which can be recovered from

$$\sup_t \hat{a}_{IJ}(t) - \inf_t \hat{a}_{IJ}(t) \leqslant \max_{\gamma\in\Gamma} \Delta s[\hat{\gamma}] - \min_{\gamma\in\Gamma} \Delta s[\hat{\gamma}], \qquad (8)$$

a direct consequence of (5). The corresponding result in Ref. [34] follows by noting that the existence of paths that realize the maximal and minimal value of Δs in the previous equation implies the existence of a circular path with entropy production equal to the right-hand side of Eq. (8). If this value is nonzero, we can conclude the existence of a hidden cycle with nonvanishing entropy production.

Third, for $I = J$ the involved trimmed paths $\hat{\gamma}$ start and end with the same transition and therefore correspond to a cycle. In this case, the bounds (5) reduce to results introduced in Ref. [28] as affinity estimators for cycles containing the transition I (but no other observed transition). We note that if one is interested in cycle affinities in particular, it is in principle possible to disregard particular observed transitions or include only particular sequences of transitions in the waiting-time distributions to obtain different bounds on cycle affinities. For example, if there are two observed transitions I and J (and their corresponding reverse), we can disregard J to obtain affinity bounds on the set of cycles that contain I irrespective of whether J is included or not. It is also possible to extract waiting-time distributions of, say, the form $\Psi_{I\to I}(t|$ contains $J)$. In this case, we could repeat the steps above to find bounds on cycles that contain both transitions I and J. The result presented here, however, enables us to treat the paths from I to J and from J to I individually, so that applying the bounds (6) or (7) will yield more resolved and therefore superior estimates.

B. Numerical illustration

We illustrate our findings for a network with the topology sketched in Fig. 2(a), which has visible transitions $I_\pm$, $J_\pm$ and transition rates as given in Appendix D 2. We select the transitions $I = I_+ = 7 \to 4$ and $J = J_+ = 9 \to 10$ and depict $\hat{a}_{I_+J_+}(t)$ as a function of the waiting time t between the two transitions in Fig. 2(b). According to the results (6) and (7), there must be one path each from state 4 to state 9, whose microscopic entropy production is bounded by $\sup_t \hat{a}_{IJ}(t)$ from below and $\inf_t \hat{a}_{IJ}(t)$ from above, respectively. We illustrate this bounding behavior, with the loopless paths γ_1, γ_2 and γ_3 as defined in Fig. 2, for the setup of Fig. 2(b), where $\hat{a}_{IJ}(t)$ bounds the microscopic entropy production $\Delta s[\gamma_1]$ from above and $\Delta s[\gamma_3]$ from below.

We assess the quality of these bounds by defining an appropriate quality factor Q, which satisfies $0 \leqslant Q \leqslant 1$ and approaches the upper bound if the corresponding estimate is tight. Additionally, it is sensible to define the quality factor in such a way that Q is invariant under constant shifts of all involved quantities. This is possible because whenever there is a unique shortest path γ_0 from I to J like $\gamma_0 = (4389)$ in

Fig. 2, we have

$$\lim_{t\to 0} \hat{a}_{IJ}(t) = \Delta s[\gamma_0]. \tag{9}$$

Intuitively, this identity states that as $t \to 0$ the probability that the hidden intermediate path between I and J is γ_0 approaches one. This reasoning can be made more rigorous by expanding $\hat{a}_{IJ}(t)$ in powers of t employing similar techniques as in Sec. IV or Ref. [28]. Thus, we can define

$$Q = \frac{\sup_t |\hat{a}_{I_+J_+}(t) - \Delta s[\gamma_1]|}{\max_{i\in\{1,2,3\}} |\Delta s[\gamma_i] - \Delta s[\gamma_1]|} \tag{10}$$

in the setup of Fig. 2, where $\gamma_0 = \gamma_1$ and Eq. (9) ensures that the numerator is operationally accessible. We note that $Q \leqslant 1$ follows from either Eq. (6) or Eq. (7), depending on whether $\sup_t \hat{a}_{IJ}(t)$ or $\inf_t \hat{a}_{IJ}(t)$ has a greater distance to $\Delta s[\gamma_1]$. In many cases including the example depicted in Fig. 2(b), the other of the two values coincides with $\lim_{t\to 0} \hat{a}_{IJ}(t)$, so that the corresponding bound is trivially satisfied.

The results of a numerical study to investigate the performance of Q are depicted in Fig. 2(c). The transition rates are randomly drawn from the distributions specified in Appendix D 2. As can be seen from the blue curve in Fig. 2(c), the average value of Q varies between $Q \simeq 0.3$ and $Q \simeq 0.6$, with on average tighter estimates when $\Delta s[\gamma_1]$ is large.

IV. SHORTEST PATHS BETWEEN VISIBLE TRANSITIONS

The waiting-time distributions $\Psi_{I\to J}(t)$ defined in Eq. (2) for transitions $I = (ij), J = (kl)$ are nonzero for all times $t > 0$ if states j and k are connected in the hidden graph. For such transitions I and J, we define the two topological quantities $N_{1,IJ}$ and $N_{2,IJ}$. These quantities represent the number of hidden transitions along the shortest and second-shortest paths between I and J, which we require to be self-avoiding. Such self-avoiding paths naturally contain neither loops nor any repeated transition. This property is inherent to the shortest path. It is a necessary condition that, in particular, excludes a transition followed by its reverse from the second-shortest path, so that it corresponds to a distinct path in the underlying graph. Otherwise, the value $N_{2,IJ}$ could not exceed $N_{1,IJ} + 2$, providing no further insight.

The sum of path weights of all trajectories that start in state i at time $t = 0$ and end in the neighboring state j at time t satisfies $p(j, t|i, t = 0) = k_{ij}t + O(t)$. For a path with N_1 transitions between j and l, the corresponding probability is proportional to t^{N_1} in the short-time limit. Longer paths contribute to terms of higher order in t, while sojourn times enter the path weights in exponential factors. Consequently, with a shortest path of N_1 transitions between j and l, we obtain $p(l, t|j, t = 0) \sim t^{N_1}[1 + O(t)]$. Since $\Psi_{I\to J}(t)/k_{kl} = p(l, t|j, t = 0)$, only the shortest path between I and J contributes to $\Psi_{I\to J}(t)$ in the short-time limit $t \to 0$, which leads to the number of hidden transitions

$$N_{1,IJ} = \lim_{t\to 0} \left(t \frac{\mathrm{d}}{\mathrm{d}t} \ln \Psi_{I\to J}(t) \right) \tag{11}$$

along the shortest path from I to J [28].

Next, we focus on the short-time behavior of the quantity $\hat{a}_{IJ}(t)$ defined in (3). For short times, $\hat{a}_{IJ}(t) \sim \hat{a}_{IJ}(0) + ct^{u_{IJ}}$ with some real number c, as illustrated in Fig. 1, which motivates the definition

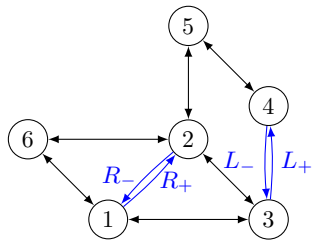


FIG. 3. Multicyclic graph of a partially accessible Markov network. Blue, labeled transitions $R_\pm$, $L_\pm$ are observable, whereas states and remaining transitions are hidden.

$$u_{IJ} \equiv \lim_{t\to 0} \left(t \frac{\mathrm{d}}{\mathrm{d}t} \ln |\hat{a}_{IJ}(t) - \hat{a}_{IJ}(0)| \right), \tag{12}$$

where the first term of definition (3) drops out. This quantity u_{IJ} is formally ill-defined for $\hat{a}_{IJ}(t) = \text{const}$, in which case we set $u_{IJ} \equiv 0$.

For the remainder of this section, we assume that paths from I to J do not contain a part of a cycle with vanishing affinity. Within this class, the number of hidden transitions $N_{2,IJ}$ along the second-shortest path between I and J is given by

$$N_{2,IJ} = u_{IJ} + N_{1,IJ} \tag{13}$$

in the following cases [28].

First, this holds true for $u_{IJ} \geqslant 2$, which applies, e.g., to the network shown in Fig. 1.

Second, for $u_{IJ} = 1$ and $N_{1,IJ} \geqslant 1$, Eq. (13) yields the correct length $N_{2,IJ}$ or the shortest path between I and J is degenerate. In the latter case, the degenerate paths form a cycle with nonzero affinity, such that for $N_{1,IJ} \geqslant 2$ sojourn times in states along the distinct shortest paths lead to a term in $\hat{a}_{IJ}(t)$ that is proportional to $t^{N_{1,IJ}+1}$. Since then the same power arises from a second-shortest path with $N_{2,IJ} = u_{IJ} + N_{1,IJ}$, this analysis cannot distinguish these two different topologies, as is the case, e.g., for $I_+ \to J_+$, $I_- \to J_-$ and $I_+ \to J_-$ in Fig. 2.

Finally, $u_{IJ} = 0$, which arises from a time-independent $\hat{a}_{IJ}(t)$, implies that there is no second-shortest self-avoiding path between I and J. For example, this is the case in Fig. 3 for $I = L_+$ and $J = R_-$. Note, however, that this conclusion cannot be drawn if we drop the assumption that paths must not contain parts of cycles with vanishing affinity.

Two additional features will become relevant below. First, $N_{i,IJ} = N_{i,\bar{J}\bar{I}}$ for $i = 1, 2$ and $u_{IJ} = u_{\bar{J}\bar{I}}$ because the same path is used in both forward and backward direction. Second, treating all edges from a set K as hidden can alter the shortest hidden paths between two visible transitions by creating a shortest or a second-shortest, hidden self-avoiding path that was previously interrupted by a visible link. Doing so translates to an observer to whom edges from the set K are invisible or who ignores registered transitions corresponding to edges within K, whereas the underlying dynamics remains unchanged in both interpretations. Hence, we define $N_{1,IJ\setminus K}$, $u_{IJ\setminus K}$ and $N_{2,IJ\setminus K}$ analogously to Eq. (11)–(13) for observations in which the transitions included in the set K

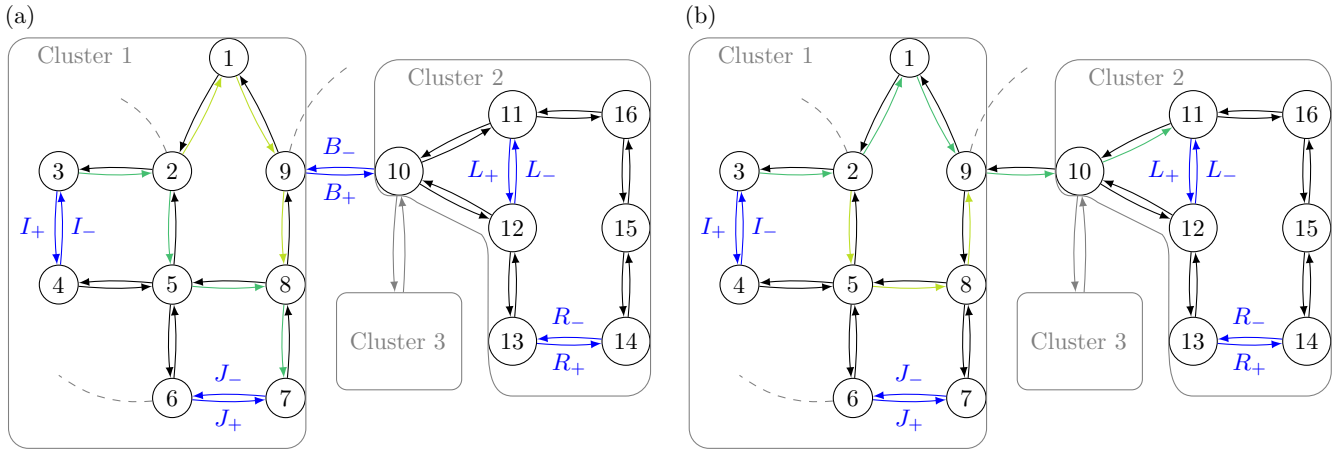


FIG. 4. Subnetwork with three clusters of states connected by bridges. All states and edges except the blue, labeled ones are hidden. Dashed, gray lines indicate additional paths to arbitrary subgraphs that are within cluster 1 and outside the drawn clusters, respectively. (a) Irrespective of whether we can observe edge pair $B_\pm$, which is the bridge between clusters 1 and 2, the shortest path connecting I_- and J_- is $\xrightarrow{I_-} 3 \to 2 \to 5 \to 8 \to 7 \xrightarrow{J_-}$ shown in teal. The second-shortest path is $\xrightarrow{I_-} 3 \to 2 \to 1 \to 9 \to 8 \to 7 \xrightarrow{J_-}$ shown in olive green. Their length differs by $N_{2,I_-J_-} - N_{1,I_-J_-} = 5 - 4 = 1$ hidden transition. (b) The shortest and the second-shortest path between I_- and L_+ consist of teal as well as of olive green edges, respectively. Both contain the bridge between clusters 1 and 2, and the shortest partial path within cluster 2, while their partial paths (between states 2 and 9) in cluster 1 are distinct.

are treated as hidden. As a consequence, the values of these quantities can be decreased when compared to the respective original quantities $N_{1,IJ}$, u_{IJ} and $N_{2,IJ}$. For example, ignoring $R_\pm$ transitions in observations of the network depicted in Fig. 3 changes $N_{2,L_\pm L_\pm} = 5$ (for the second-shortest path $\xrightarrow{L_+} 4 \to 5 \to 2 \to 6 \to 1 \to 3 \xrightarrow{L_+}$) to $N_{2,L_+L_+\setminus R_\pm} = 4$ ($\xrightarrow{L_+} 4 \to 5 \to 2 \to 1 \to 3 \xrightarrow{L_+}$).

V. FOOTPRINTS OF CLUSTERS: THE PAIR RULE

In this section, we assume a network of states that can be characterized as a tree of clusters; see, e.g., Fig. 4(a). A cluster consists of states connected by paths. Two clusters are connected by a bridge, which means they are unconnected after removing the bridge. A genuine bridge, consisting of a pair of edges $B_\pm$, appears in Fig. 4(a). Within this paper, a bridge could also be larger and consist of a self-avoiding path of n links. A degenerate bridge is a single state. The tree-like topology on the level of clusters means that the network obtained by treating all clusters as states does not contain any cycles.

A visible bridge link like $B_\pm$ in Fig. 4(a) allows us to identify clusters in a partially visible Markov network. Such links $\pm$ are not a part of any cycle within the graph meaning that both waiting-time distributions $\Psi_{+\to+}(t)$ and $\Psi_{-\to-}(t)$ vanish identically. While this condition uniquely characterizes such situations, identifying clusters without having access to visible bridge links is more involved as we will discuss now.

In preparation for this more general case of inference, we first derive a graph-theoretical fact. For any pair of visible transitions $J_\pm$ and $L_\pm$, consider in each of the four lines

$$N_{2,J_+L_s} - N_{1,J_+L_s}, \tag{14a}$$

$$N_{2,J_-L_s} - N_{1,J_-L_s}, \tag{14b}$$

$$N_{2,J_sL_+} - N_{1,J_sL_+}, \tag{14c}$$

and

$$N_{2,J_sL_-} - N_{1,J_sL_-} \tag{14d}$$

these differences for $s = +$ and $s = -$, each of which we will call a pair of differences in the following. If in none of these four pairs the two differences are equal, we can be sure that the two links belong to the same cluster. Likewise, if the two links belong to different clusters, at least in one pair the two differences have to be equal. Before we prove this pair rule, as we dub it, we illustrate this criterion with the graph shown in Fig. 4.

In this network, we assume B_+ and B_- to be hidden in the following. First, consider the edges $I_\pm$ and $J_\pm$. The shortest and second-shortest path connecting I_- and J_- is highlighted in Fig. 4(a) in teal and olive green, respectively. We thus get the crucial difference

$$N_{2,I_-J_-} - N_{1,I_-J_-} = 5 - 4 = 1. \tag{15}$$

Similarly, we get

$$N_{2,I_-J_+} - N_{1,I_-J_+} = 6 - 3 = 3, \tag{16}$$

noting that the two differences in this pair are distinct. Fixing I_+ as the first transition, we get

$$N_{2,I_+J_-} - N_{1,I_+J_-} = 6 - 3 = 3. \tag{17}$$

For the sequence $I_+ \to J_+$, the second-shortest path does not exist. In this case, we assign the value zero to the difference

$$N_{2,I_+J_+} - N_{1,I_+J_+} \equiv 0. \tag{18}$$

Again, we see that the differences in Eqs. (17) and (18) are distinct. Likewise, if we keep the second visible tranisiton fixed and change the first one, i.e., $N_{2,I_sJ_+} - N_{1,I_sJ_+}$ and $N_{2,I_sJ_-} - N_{1,I_sJ_-}$ for $s = \pm$, we find that in none of the resulting two pairs with fixed second transition do the differences match. Since I and J are in the same cluster, the differences in

none of the four pairs match, which is in agreement with the pair rule stated above.

Alternatively, if we select the edge pairs $I_\pm$ and $L_\pm$, which are in different clusters, we get for the first pair

$$N_{2,I_-L_-} - N_{1,I_-L_-} = 6 - 5 = 1,$$
$$N_{2,I_-L_+} - N_{1,I_-L_+} = 6 - 5 = 1. \tag{19}$$

These two differences are the same, since both shortest paths contain the sequence $3 \to 2 \to 1 \to 9$ in Cluster 1, and both second-shortest paths differ from the shortest path only within Cluster 1 by containing the sequence $3 \to 2 \to 5 \to 8 \to 9$ instead. We refer to such parts of shortest paths that lie within one cluster as the shortest partial path and adopt an analogous definition for the second-shortest partial path. The remaining parts of the shortest paths, i.e., the bridge and the partial paths in Cluster 2, corresponding to each difference are identical and thus do not contribute to it, as shown in Fig. 4(b). We will now show that such an equality between differences in one of the pairs (14a) to (14d) has to occur whenever the chosen pair of visible transitions is in different clusters.

In a general network containing clusters, the second-shortest path between visible edges J_j, L_l with $j, l \in \{+, -\}$ located in different clusters differs from their shortest path within one of the clusters by the self-avoiding path between bridge and visible transition. Specifically, it contains the second-shortest partial path, which differs from the corresponding shortest partial path by the fewest hidden edges. The number of these hidden edges equals the difference $N_{2,J_jL_l} - N_{1,J_jL_l}$. Since there are four shortest paths between $J_\pm$ and $L_\pm$ in total, and one of the differences in partial paths is the smallest, this minimal difference equals two of the four differences $N_{2,J_jL_l} - N_{1,J_jL_l}$, thus forming a pair. Additionally, the transition that remains fixed within the pair indicates the cluster in which the smallest difference in partial paths between the two visible transitions lies. Using similar reasoning, if there are two second-smallest differences in partial paths or both second-shortest partial paths lie in the same cluster, two pairs exist. An example is the combination $I_\pm, L_\pm$ with hidden $B_\pm$ in Fig. 4(b), where the second-shortest partial paths are in Cluster 1. Other relations between the values of the differences in partial paths lead to a triplet or to two equal pairs.

Consequently, the pair rule yields a sufficient criterion to rule out that two links are in different clusters. Conversely, a necessary condition for two links to be in different clusters is the existence of equal differences in at least one such pair of the pair rule. This pair rule thus provides insight into the global structure of a graph.

VI. RECONSTRUCTING A MINIMAL GRAPH

The ability to infer topological information about a Markov network based on waiting times between visible transitions provokes the question of how to reconstruct a minimal graph that is compatible with the observations. But what is a minimal graph of such a network that we might want to construct? We define the largest subgraphs an observer can reconstruct with the tools of Secs. IV and V (up to relabeling states) as a realization of the minimal graph. If this realization is unique it is the minimal graph.

There are three motifs that can be added to a minimal graph without getting into conflict with observations based on the topological information our methods yield. First, one can always connect otherwise unconnected subgraphs that contain no visible edges to the graph via a hidden bridge as defined in Sec. V. Second, one can always split a hidden edge into multiple hidden channels between two neighboring states. Third, one can always add paths leading to cycles with vanishing affinity, unless they introduce a new shortest path that decreases some of the $N_{1,\dots}$. In the following we will focus on the realizations of the minimal graph without such additional elements. Yet, there may be restrictions or indications that additional extensions are required, the graphical representation of which are then part of the minimal graph. In summary, the topology of the inferred graph will match the observed data, while in general the full underlying graph may remain unknown.

Building on operationally accessible knowledge about shortest paths between edge pairs, in particular the quantities $N_{1,\dots}$ and $u_{\dots}$ as discussed in Sec. IV, we present strategies and tools to reconstruct a minimal graph or realizations thereof for general, partially accessible Markov networks. First, we discuss the case of one visible pair of edges in Sec. VI A. Second, we illustrate two examples with multiple visible edge pairs, one with and one without distinct clusters, in Secs. VI B and VI C, respectively. Finally, we present a general algorithm in Sec. VI D.

In all cases, we assume the observer has already determined the smallest numbers of hidden transitions between any two visible ones as discussed in Sec. IV. Moreover, we again note that hidden paths with the same entropy production as the shortest path between two visible transitions are not part of a minimal graph, as they lead to a cycle with vanishing affinity. Therefore, we can use Eqs. (12) and (13) to determine the hidden length of the second-shortest paths between two visible transitions I, J in the minimal graph, relying on the results except for the case of $u_{IJ} = 1$ with $N_{1,IJ} \geqslant 2$.

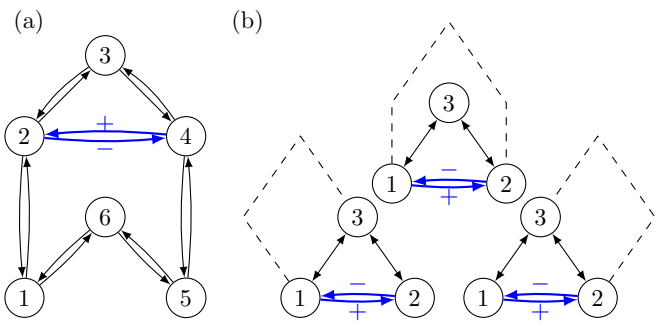


FIG. 5. A graph and realizations of its minimal graph. Except for the labeled visible edges (blue), all states and edges are hidden. (a) Multicyclic graph with $N_{1,++} = 2$ and $N_{2,++} = 4$. (b) The three realizations of a minimal graph for the graph in (a). The realizations consist of a three-state unicycle with labeled visible edges in blue, double-headed arrows as hidden edge pairs and a dashed extension with vertices as states that potentially exist in the true graph.

TABLE I. Inferred quantities associated with the number of hidden transitions along shortest paths between visible edges in the network in Fig. 3. One of two (by symmetry) equivalent combinations of visible edges IJ and, if applicable, the set K of visible edges treated as hidden precedes its value of $N_{1,\dots}$ or $u_{\dots} + N_{1,\dots}$ in the syntax $IJ \setminus K$ introduced in Sec. IV.

$N_{1,\dots}$		$N_{1,\dots}$		$u_{\dots} + N_{1,\dots}$		$u_{\dots} + N_{1,\dots}$	
L_+L_+	3	$L_+L_+ \setminus R_\pm$	3	L_+L_+	5	$L_+L_+ \setminus R_\pm$	4
R_+R_+	2	$R_+R_+ \setminus L_\pm$	2	R_+R_+	3	$R_+R_+ \setminus L_\pm$	3
L_+R_+	4			L_+R_+	5		
L_+R_-	2			L_+R_-	2		
L_-R_+	1			L_-R_+	3		
L_-R_-	1			L_-R_-	3		

A. One visible pair of edges

For observations of a single pair of edges, like $+$ and $-$ in Fig. 5(a), we first note that $N_{1,++} > 1$, because otherwise a cycle containing only the two states connected by a visible and a hidden link exists. In such a case with visible and hidden channels between states our results can be applied in a similar way, but we will not investigate this case explicitly here.

Proceeding with the case that $N_{1,++} > 1$, drawing the shortest cycle of the pair $\pm$ completes the graph that can be reconstructed with certainty. Since there is no unique way to append the second-shortest cycle of $\pm$, each version of the graph that includes a realization of it is a possible extended minimal graph. Assume, for example, a network as shown in Fig. 5(a) where $N_{1,++} = 2$ and $N_{2,++} = 4$. Figure 5(b) displays the three possible realizations of the true graph.

This introductory example demonstrates that a minimal graph need not exist. Instead, we obtain different possible realizations of which one graph is contained in or, in this case, coincides with the underlying graph.

B. Illustrative example I: A cycle-based approach for multiple observed edges

In this example, we reconstruct the minimal graph of the Markov network shown in Fig. 3 by iteratively adding paths and cycles to an initial cycle. We assume the perspective of an observer who has listed the inferred numbers of hidden transitions along the two shortest paths between visible transitions in Table I. Based on this information, the reconstruction proceeds as follows in three steps, illustrated in Fig. 6.

(1) The shortest cycle inferable from Table I arises from the sequence $R_+ \to R_+$ with $N_{1,R_+R_+} = 2$. It includes $R_\pm$ and two hidden transitions. The state between these hidden transitions connects this cycle to the visible edge pair $L_\pm$ as a direct consequence of $N_{1,L_-R_\pm} = 1$. Thus, we draw this cycle and both visible edge pairs in Fig. 6(a), where we also indicate all possible ways to add the shortest cycle that contains $L_\pm$.

(2) We need to connect states 2 and 4 via two hidden edge pairs due to $N_{1,L_+R_-} = 2$. This path, $2 \to 5 \to 4$, creates a fitting shortest cycle containing $L_\pm$. The two alternative ways to draw a shortest cycle of $L_\pm$ fail to preserve $u_{L_+R_-} = 0$ as shown in Fig. 6(b). Moreover, introducing a path of two hidden transitions between states 1 and 4 violates $N_{1,L_+R_+} = 4$. After rejecting these incompatible realizations, we proceed with the graph displayed in Fig. 6(c).

(3) The constructed graph in Fig. 6(c) now agrees with all values for $N_{1,\dots}$ listed in Table I but at this point lacks appropriate second-shortest paths, in particular the second-shortest cycle containing $L_\pm$. This cycle has to comprise $u_{L_+L_+} + N_{1,L_+L_+} = N_{2,L_+L_+} = 5$ hidden transitions, for which there are *a priori* various realizations. Figure 6(c) indicates the realizations that we cannot rule out with the previous considerations. Since extensions along the path between states 2 and 4 violate $u_{L_+R_-} = 0$, a path of two hidden transitions between states 1 and 2 is the only realization that is consistent with all data given in Table I. We thus find that $N_{2,L_+R_+} = N_{1,L_+R_+} = 4$ holds, since the corresponding shortest and second-shortest path contain the same number of hidden transitions. This is different to what Table I suggests, i.e., different to $u_{L_+R_+} + N_{1,L_+R_+} = 1 + N_{1,L_+R_+} = N_{2,L_+R_+}$. Analogously, we find that $N_{2,R_+R_+} = N_{2,R_+R_+\setminus L_\pm} = N_{1,R_+R_+} = 2$ holds. Finally, Fig. 6(d) displays the reconstructed minimal graph, which matches the original graph from Fig. 3.

Thus, in this case, the network with six states and eight edge pairs in total can be reconstructed fully based on the observation of waiting times between combinations of the four transitions that are part of the two visible links.

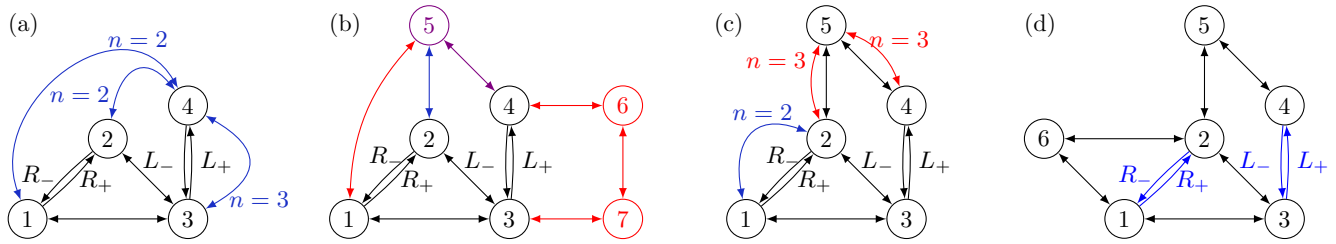


FIG. 6. Construction of a minimal graph. The procedure relies on the inferred number of hidden transitions along shortest paths between visible edges as given in Table I. Visible edge pairs are labeled, while hidden links are shown as double-headed arrows. (a) The three ways to extend the shortest cycle containing $R_\pm$ and its connection to $L_\pm$ with the shortest cycle that includes the latter edge pair. Each extension and its number n of required hidden transitions to achieve $N_{1,L_+L_+} = 3$ are highlighted in blue. (b) Concrete realizations of extensions in (a). The only allowed path is displayed in blue and violet while red realizations fail to respect $u_{L_+R_-} = 0$ or $N_{1,L_+R_+} = 4$. (c) The three ways to extend the unique, compatible graph from (b) with the second-shortest cycle containing $L_\pm$ and $N_{2,L_+L_+} = u_{L_+L_+} + N_{1,L_+L_+} = 5$ hidden links that have no similarity with rejected realizations in (b). Only the blue path of $n = 2$ hidden transitions is compatible with the values listed in Table I. (d) Final minimal graph with visible edges in blue. This graph follows after rejecting red extensions in (c) and is the same as the original graph shown in Fig. 3.

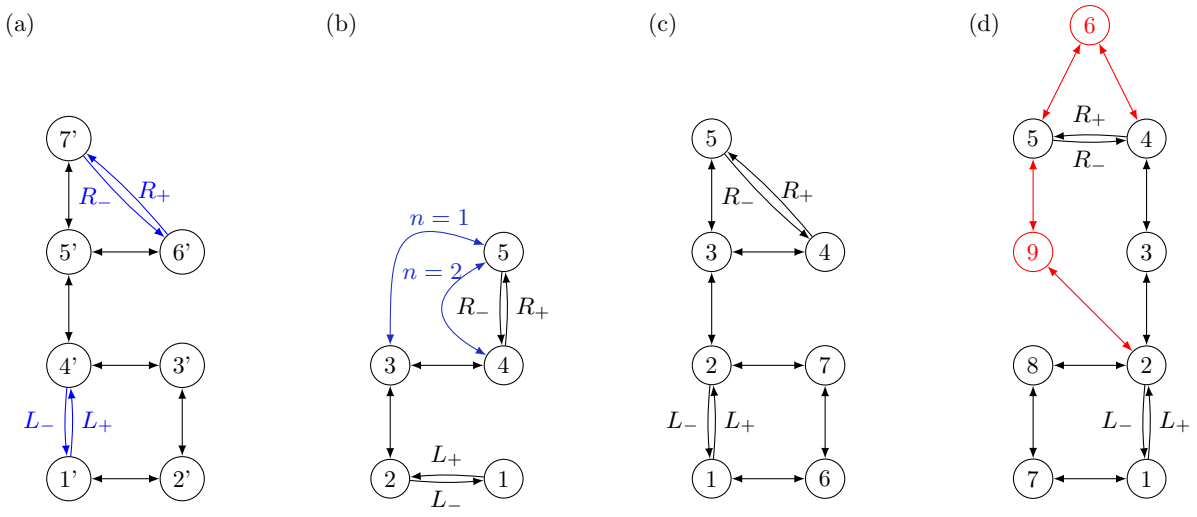


FIG. 7. Construction of minimal graphs for a graph with two clusters. To stress the unknown character, the states of the underlying graph are labeled with a prime, whereas in the reconstruction the states are labeled with consecutive numbers. (a) Graph with visible transitions $R_\pm$, $L_\pm$ that leads to the inferred data listed in Table II. Using this data, we construct minimal graphs in (b) to (d), which demonstrates the branching behavior of this approach leading to multiple realizations for a graph. (b) A shortest hidden path between $L_\pm$ and $R_\pm$ with $N_{1,L_+R_+} = 2$. The blue labeled arrows indicate the two possible ways to draw the shortest cycle that contains $R_\pm$ and $N_{1,R_+R_+} = 2$, with $n = 1, 2$ additional, hidden transitions. (c) Realization of a minimal graph with $n = 1$ from (b) in which the shortest cycle containing $L_\pm$ with $N_{1,L_+L_+} = 3$ must not include states 4, 5, and 3, since a direct link between states 1 and 4, 5 as well as between 6 and 3 would contradict $N_{1,L_-R_+} = 5$. (d) Realization of a minimal graph with $n = 2$ in (b) with shortest cycle containing $R_\pm$ leading to $N_{1,R_+R_+} = 2$ and shortest hidden path between L_+ and R_- leading to $N_{1,L_+R_-} = 2$ in red. The red paths form a second-shortest cycle including R_+ and a second-shortest path for the four sequences $L_\pm \to R_\pm$ that are in conflict with the corresponding $u_{\dots} = 0$. Alternatively, the affinity-based criterion discussed in Sec. C 2 helps to rule out this realization since all $\hat{a}_{\dots}(t)$ are time-independent such that the graph in (c) remains as the unique minimal graph that is the same as the graph in (a) after relabeling states.

For more complicated networks that contain clusters and bridges, the steps within this approach often result in multiple putative graphs. Each of these graphs requires further extension within the method. In such cases, the method branches. When it comes to connecting potential clusters, we extend and modify this method by focusing on paths rather than cycles. This adjustment makes the branching behavior more tractable, as will be illustrated in the following example.

C. Illustrative example II: A path-based approach for multiple observed edges

In our second example, we focus on paths between distinct visible edge pairs, which in this case are key to connect visible edge pairs from different clusters. This example also elucidates the type of branching behavior that results in different compatible graphs. We consider the graph shown in Fig. 7(a), which contains two clusters. The information on shortest paths that an observer can infer is given in Table II. For this network, the observer finds that $u_{\dots} = 0$ for all sequences of transitions. Thus, the minimal graph will contain no second-shortest paths.

(1) The sequence $L_+ \to R_+$ has one of the two equally shortest paths with $N_{1,L_+R_+} = 2 = N_{1,L_+R_-}$ hidden links between the two links $L_\pm$, $R_\pm$, as given in the second column of Table II. We therefore start drawing the graph with this sequence, as depicted in Fig. 7(b).

(2) The shortest cycle including $R_\pm$ and $N_{1,R_+R_+} = 2$ hidden links can be added in the two ways indicated in Fig. 7(b). We start with the realization featuring $n = 1$ hidden link between states 3 and 5. Adding the shortest cycle that contains $L_\pm$ and $N_{1,L_+L_+} = 3$ hidden links, as displayed in Fig. 7(c), completes an allowed minimal graph. In particular, this graph includes neither shorter self-avoiding paths than given by the values in Table II nor second-shortest paths. Other ways to draw this cycle contradict $N_{1,L_-R_+} = 5$. Therefore, the only resulting graph matches the original one in Fig. 7(a) up to state relabeling.

A putative further realization uses the $n = 2$ option from Fig. 7(b). This realization again requires connecting states 1 and 2 as shown in Fig. 7(c) to the unique shortest cycle containing $L_\pm$, and ensuring that second-shortest cycles that contradict Table II are not introduced. The value $N_{1,L_+R_-} = 2$ requires a separate path of two hidden transitions between

TABLE II. Inferred numbers of hidden transitions along shortest paths between two visible transitions in a graph as shown in Fig. 7(a). The combination of visible edges IJ and, if applicable, the set K of visible edges treated as hidden precedes its value of $N_{1,\dots}$ or $u_{\dots} + N_{1,\dots}$ in the syntax $IJ \setminus K$ introduced in Sec. IV.

$N_{1,\dots}$		$N_{1,\dots}$	
L_+L_+	3	L_+R_+	2
$L_+L_+ \setminus R_\pm$	3	L_+R_-	2
R_+R_+	2	L_-R_+	5
$R_+R_+ \setminus L_\pm$	2	L_-R_-	5

L_+ and R_- like in Fig. 7(d), but this introduces an unwanted second-shortest cycle containing $R_\pm$. Drawing this path would also conflict with $u_{\dots} = 0$ for the four sequences $L_\pm \to R_\pm$ because they have no second-shortest paths. Thus, this realization is incompatible with the observations and must be discarded.

The approach described above is not the only way to obtain the graph that yields the desired values of $N_{1,\dots}$ as given in Table II and $u_{\dots} = 0$. We could alternatively use a criterion discussed in detail in Sec. C 2, which allows us to restrict the set of compatible graphs by using methods similar to those described in Sec. III. The reasoning is based on inferring cycle affinities and entropy production along microscopic paths and discarding the realizations where these quantities lead to inconsistent results.

In conclusion, we are able to find a unique minimal graph that, in this case, coincides with the original graph after relabeling states. This example also demonstrates that even if we obtain different possible realizations of the minimal graph in an intermediate step, it is possible that such realizations have to be discarded at a later stage when they turn out to be inconsistent.

D. General method to reconstruct realizations of a minimal graph

In this section, we compile our previous heuristic insights into an algorithm, which is illustrated as a flowchart in Fig. 8.

We can conceptualize the algorithm as comprising two distinct components. The first part encompasses the first three steps in the algorithm until Result B and aims at identifying putative clusters (PCs) based on the pair rule of Sec. V. These clusters are connected before we proceed with the connections within a PC. This approach proved useful for networks that feature bridges or bottlenecks like the one previously discussed in Sec. VI C. It is worth noting that, since the pair rule only provides a necessary criterion to identify multiple clusters, the structure of PCs may change as additional information is added to the subgraph later in the algorithm. For example, if it turns out that two PCs are connected by not only one bridge, these two PCs have to be combined into a single PC, which also entails checking whether there are additional cross-connections between the previously separate clusters.

The second part of the algorithm utilizes this preliminary structure to systematically include information about first the shortest and then the second-shortest connections. This procedure repeatedly calls the subroutine depicted in Fig. 9. In this subroutine we encounter the peculiar branching behavior that was already present in the previous examples. It is important to note that the algorithm must be continued for each individual putative realization, because it is possible that such branches can be ruled out at some later point in the algorithm, as we encountered in the example of Sec. VI C. As one would expect already from the introductory example in Sec. VI A, the algorithm yields not a single minimal graph but different possible ones in the general case.

A more formal presentation of the algorithm is found as pseudocode in Sec. B, which also discusses particularly subtle aspects in more detail.

VII. DISCUSSION: CONCEPTUAL APPROACHES AND THEIR LIMITATIONS

This work focuses on what might be deemed a thermodynamic approach to inference of an underlying graph. The theme common to the methods described here is, apart from assuming that transitions are the elementary observable, the conceptual focus on $\hat{a}_{IJ}(t)$. This measure of broken detailed balance that can be given a precise thermodynamic interpretation as a coarse-grained entropy production [34]. In this sense, we provide a quantitative extension of previous studies that relate observed broken time-reversal symmetry, a qualitative, binary property, to topological aspects of the underlying hidden layer [41–43].

An important consequence is that the methods presented here are insensitive to a number of operations that do not change nonequilibrium characteristics, which includes the addition of equilibrium cycles, tree-like appendages or even entire clusters if such clusters do not contain a single visible transition and connect to the remaining network only via a bridge. Additionally, a hidden edge could always be split into multiple channels between two states. Due to such shortcomings, one might argue that the thermodynamic approach is inferior to, say, Markov state modeling [44], because the reconstruction of an underlying model is at best possible in a "minimal" sense, i.e., up to in this approach invisible additions.

However, if we are particularly interested in the nonequilibrium aspects of a given model, insensitivity to changes in the nondriven parts of the network may be a desirable rather than a detrimental feature. To illustrate this point, let us consider the heat shock protein Hsp90 as a concrete example. This protein displays nonequilibrium behavior in the presence of ATP and suitable cochaperones and is therefore interesting from a thermodynamic point of view [45], but the presence of strong memory effects in the observed dynamics render a direct description in terms of a hidden Markov model difficult and potentially even misleading [46]. In such a scenario, our thermodynamic tools offer insights into the parts of the underlying model that couple to the external driving. In combination with other constructive methods like hidden Markov modeling, our tools can also be understood as a set of operationally verifiable criteria to check whether a proposed model allows for a consistent description from a thermodynamic point of view.

In the following, we comment on the limitations of our methods in more detail. These remarks serve as possible starting points for improvements and refinements of our methods that may be the subject of future work.

A. Thermodynamic inference of microscopic paths

In Sec. III we present a set of inequalities through which we can infer the existence of microscopic paths with dissipation greater or smaller than an operationally accessible threshold. Focusing on properties of the model on the underlying Markovian level, these relations complement a number of results regarding thermodynamic properties of the transition-based model on the coarse-grained level [28,29,33–35,47].

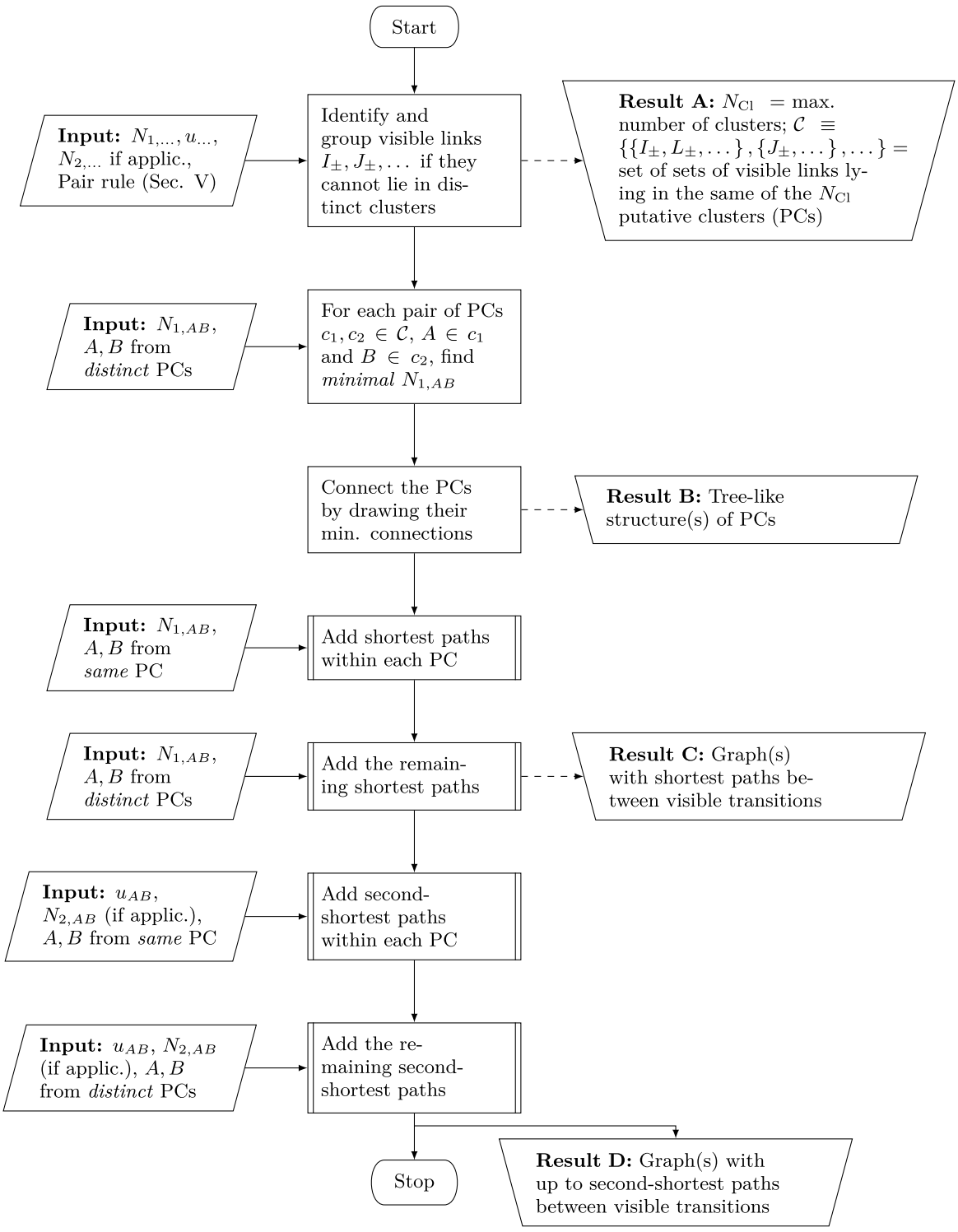


FIG. 8. An algorithm to reconstruct realizations of a minimal graph. The procedure takes the inferred values of $N_{1,\ldots}$, $u_{\ldots}$ and, if applicable, of $N_{2,\ldots}$ along with the pair rule from Sec. V as its input. It is possible that the algorithm branches, therefore it may generate multiple putative realizations of the minimal graph in the general case. The outlined procedure has to be followed for every realization individually in this case. For convenience, we list four intermediate results A to D, resulting in a four-block structure. The first block A yields the maximum number N_{Cl} of putative clusters (PCs) and a set $\mathcal{C}$ containing sets of visible links that are in the same PC. Starting in the line below result A, we connect the PCs in block B via the paths with the minimal $N_{1,\ldots}$ between each pair of PCs. The result are realizations of graphs with tree-like topology on the level of PCs. In the last two blocks, we repeatedly call the subroutine defined in flowchart Fig. 9, which is indicated by the box with double vertical lines. Explicitly given inputs define the task described in the label of the subroutine, which extends putative realizations of a minimal graph with given input. Block C generates shortest paths between all visible transitions in all putative realizations, while ensuring that they respect all relevant $N_{1,\ldots}$ and $u_{\ldots}$. Note that checking for additional realizations between visible transitions is crucial if two PCs are merged. Block D includes the analogous procedure for the second-shortest connections.

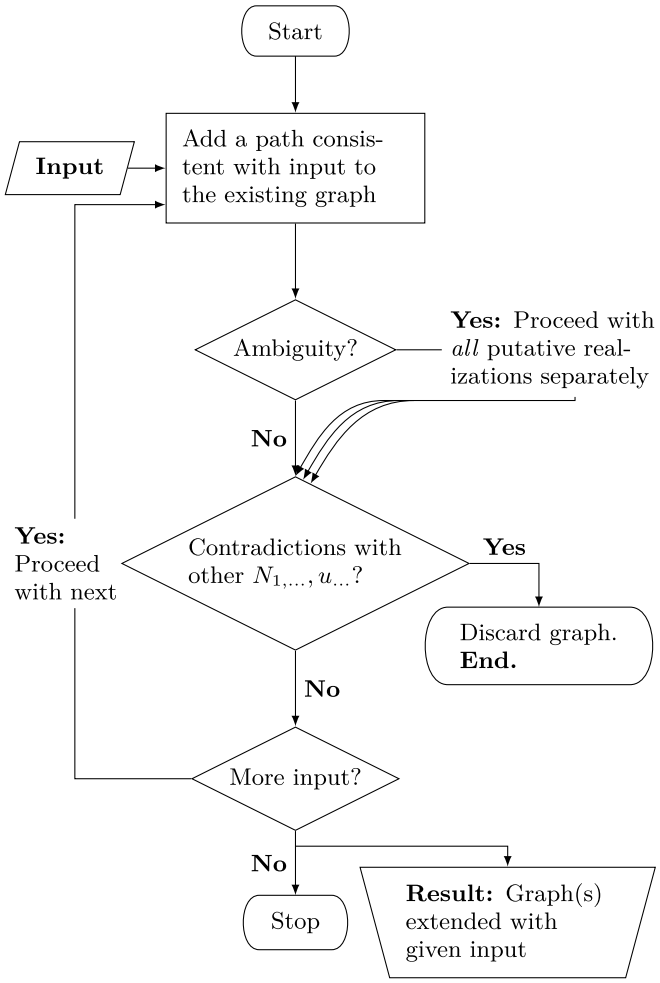


FIG. 9. The subroutine used in Fig. 8. The explicitly given input of the subroutine defines its task and its label in flowchart Fig. 8, but all $N_{1,\dots}, u_{\dots}$ are implicitly used as input when checking for contradictions. Based on the explicitly given input, the subroutine adds paths to each putative realization. If multiple realizations are possible, we proceed with each putative realization and corresponding graph separately. Realizations that do not respect all $N_{1,\dots}$ and $u_{\dots}$ are discarded. The subroutine ultimately returns all resulting putative realizations, now extended by the given input.

The main difficulty in applying these results lies in identifying an appropriate underlying Markovian layer to which these results can be applied. From a theoretical point of view, it is necessary that the dynamics and energetics of the underlying Markov model are related as described by the laws of stochastic thermodynamics [3]. In practice, such insights require knowledge about the physical coupling and energy transduction between the degrees of freedom that comprise the system and its environment. A promising example where such methods might be useful are molecular motors, where microscopic models that describe their energetics adequately are well known [48–50]. In such a case, we might speculate whether additional insights into the energetics (e.g., that cycle affinities are integer multiples of the free energy available through consumption of one ATP molecule) allow even stronger predictions about the microscopic model (e.g., the existence of a microscopic path along which one or several ATP molecules are consumed).

B. Number of hidden states along shortest paths

Our subsequent, more structural results are based on the observation that the short-time limit of waiting-time distributions contains information about the number of hidden intermediate states as described quantitatively in Sec. IV. From a practical standpoint, a significant obstacle may be to first acquire sufficient statistics to sample a waiting-time distribution and subsequently extract its short-time limit. Additionally, extracting the number of hidden states in the second-shortest cycle from the quantity $\hat{a}_{IJ}(t)$ defined in Eq. (12) is not always possible. As a nonequilibrium quantity with thermodynamic meaning, $\hat{a}_{IJ}(t)$ vanishes in equilibrium and is also otherwise unsensitive to some operations that do not change nonequilibrium properties of the network. More specifically, the apparent number of states along the second-shortest path does not change if one adds additional equilibrium cycles to the network, i.e., if the shortest and second-shortest hidden path produce the same amount of entropy, then the number of hidden states in the second-shortest path cannot be inferred.

C. Detection of clusters

The detection of clusters through what we have called the pair rule in Sec. V demonstrates that "local" inference methods based on shortest paths between transitions can in some cases provide insight into "global" properties of the network as well. Violation of the pair rule gives a sufficient criterion to rule out when two pairs of observed transitions lie in different clusters. However, we point out two important limitations of this approach. First, the pair rule is only a necessary criterion that the two links are located in different clusters. Second, in our reasoning we assume that if we treat the clusters as lumped states, the resulting network containing only the clusters does not contain any cycles. The design of more refined methods to detect clusters remains as a challenging open problem for thermodynamic inference, which given the previously discussed general limitations of thermodynamic inference might require a different conceptual approach.

D. Reconstruction of a minimal graph

The construction of nontrivial minimal graphs relies heavily on access to multiple observed transitions and the short-time limit of their corresponding waiting-time distributions, which are essential for inferring the number of hidden transitions along the shortest connecting paths. Assuming we have information on the number of states in both the shortest and second-shortest paths between pairs of transitions, the methods in Sec. VI aim at utilizing as many of the inferred quantities as possible in a systematic and consistent way. However, some difficulties inherent to this approach must be addressed.

The perhaps most severe problem is that in the general case the algorithm branches repeatedly as more topological information is included. Thus, one is left with not a single minimal graph but multiple possibilities which might be discarded at

some later point in the algorithm. It is generally to be expected that this branching behavior is more severe for more strongly connected graphs, i.e., graphs in which a vertex is connected to more hidden edges. In the general case, there is also no guarantee that the minimal graph is unique so that in the worst case one is left with a large number of potential minimal graphs corresponding to the different surviving branches of the algorithm.

VIII. CONCLUDING REMARKS AND OUTLOOK

This work describes different ways to utilize the observation of transition statistics in a partially accessible Markov network, but by no means exhausts all possibilities, because the statistics contains additional accessible but unused information. For example, the shape of the curve $\hat{a}_{IJ}(t)$ generally is simpler if the number of topologically distinct pathways from I to J is small, to the point that $\hat{a}_{IJ}(t)$ is constant in time if there is only one pathway from I to J. One might therefore speculate whether more complicated shapes of $\hat{a}_{IJ}(t)$ reveal additional topological data through their number of extrema, which could originate either from decaying coherent oscillations or topologically distinct hidden paths between the visible transitions I, J. In the latter case, the conjecture aligns with an observation in Ref. [28] for the case $I = J$, providing an example in which each of the aforementioned extrema appears to bound the affinity of a different cycle containing the transition I.

From the perspective of graph reconstruction as discussed in Sec. VI, it is also worth investigating other methods to infer the number of transitions along hidden pathways. This may take the form of a systematic analysis of the short-time limit, which then encodes information about successively longer paths in terms of successively higher order in time. However, such an approach faces not only conceptual limitations but also the practical challenge of extracting such information from experimental data. Nevertheless, additional structural information about path lengths is beneficial in multiple ways. First, we gain the ability to infer a larger portion of the underlying graph. Second, additional information provides additional restrictions on minimal graphs that can reduce the number of allowed realizations of graphs and therefore reduce the complexity of our proposed algorithm.

We may also speculate about other model classes beyond the case of observing transitions in the steady state. Due to the conceptual focus of our work, we assume systems with constant driving for simplicity, but the thermodynamic formalism based on waiting-time distributions can be transferred to the time-dependent case [51,52] and even to a more general class of observables beyond transitions [35]. We therefore expect that our results regarding hidden paths and graphs can be in principle generalized to such settings as well. Non-Markovian observables, such as lumped states or events whose reverse is not accessible, e.g., transitions for which only one direction is observed, comprise two classes of observables that have gained recent interest [53,54]. Another way to generalize the presented work is to allow for nonexponential dwell times within a state, which is a way to incorporate memory in the system. In this scenario, a starting point for future studies is Ref. [55], which makes use of waiting-time distributions to extract the number of hidden transitions along the shortest path between two succeeding visible states.

As a final remark, we emphasize that our techniques for graph reconstruction provide only one possible approach. Thus, our proof of concept provides a basis for further studies to design and investigate improved or even optimal algorithms to construct a minimal graph. In this context, a promising direction for future studies is the application of the proposed algorithm to complex networks in which the topology and the observed transitions are randomly selected. These studies enable the systematic assessment of the performance of the algorithm, which will assist in identifying optimal strategies for recovering topological data and constructing minimal graphs. The precise characterization of a minimal graph (or set of potential minimal graphs) that at the same time provides a thermodynamically consistent description is a challenging task that will be left for future works.

ACKNOWLEDGMENTS

We thank Julius Degünther for insightful discussions. J.v.d.M. was partially supported by JSPS KAKENHI (Grant No. 24H00833).

DATA AVAILABILITY

The data that support the findings of this article are not publicly available. The data are available from the authors upon reasonable request.

APPENDIX A: PROOF OF THE BOUNDS (5)

In this section, we prove the bound (5) in Sec. III. The proof follows a strategy similar to related results in Refs. [28,34]. To ensure a self-contained presentation, we summarize the steps in the proof that are identical to the reasoning in Ref. [34], but refer to there for more details.

We assume an underlying Markov network in a stationary state, in which several transitions are observed as described in the main text. Let γ be a microscopic trajectory that starts and ends with observed transitions I, J, respectively, contains no other visible transitions and has a total duration t. The summation over the path weight of all possible trajectories of this form yields the waiting-time distribution [28]

$$\Psi_{I\to J}(t) = \sum_{\substack{\gamma \text{ from } I \text{ to } J,\\ \text{length } t}} \mathcal{P}[\gamma|I]. \tag{A1}$$

A sum over the corresponding time-reverse paths $\tilde{\gamma}$ yields the according waiting-time distribution $\Psi_{\tilde{J}\to\tilde{I}}(t)$. The crucial idea of the proof is to introduce a different involution $\mathcal{R} : \gamma \mapsto \mathcal{R}\gamma$ which bijectively maps paths from I to J of length t to paths from $\widetilde{J}$ to $\widetilde{I}$ with the same duration t, so that

$$\Psi_{\tilde{J}\to\tilde{I}}(t) = \sum_{\substack{\gamma \text{ from } \tilde{J} \text{ to } \tilde{I},\\ \text{length } t}} \mathcal{P}[\gamma|\tilde{J}] = \sum_{\substack{\gamma \text{ from } I \text{ to } J,\\ \text{length } t}} \mathcal{P}[\mathcal{R}\gamma|\tilde{J}]. \tag{A2}$$

In this case, we specify $\mathcal{R}$ as the ordinary time reversal whenever γ is a trimmed path, i.e., whenever γ does not contain any cycles. If the unobserved part of γ between I and J visits any state more than once, i.e., if γ contains cycles, these cycles are

not reversed, but are traveled in the same direction for both γ and $\mathcal{R}\gamma$. For example, the trajectories

$$\begin{aligned}\gamma &= \overset{I}{\to} 4 \to 3 \to 2 \to 4 \to 3 \to 8 \to 6 \to 8 \to 9 \overset{J}{\to} \text{ and}\\ \hat{\gamma} &= \overset{I}{\to} 4 \qquad\qquad \to 3 \to 8 \qquad\qquad \to 9 \overset{J}{\to}\end{aligned} \tag{A3}$$

get mapped to

$$\begin{aligned}\mathcal{R}\hat{\gamma} &= \overset{\tilde{J}}{\to} 9 \qquad\qquad \to 8 \to 3 \qquad\qquad \to 4 \overset{\tilde{I}}{\to}\\ \mathcal{R}\gamma &= \overset{\tilde{J}}{\to} 9 \to 8 \to 6 \to 8 \to 3 \to 4 \to 3 \to 2 \to 4 \overset{\tilde{I}}{\to},\end{aligned} \tag{A4}$$

which clarifies that $\mathcal{R}$ can be understood as "taking out all cycles, reversing the path, then restoring all cycles in original direction." The operation $\mathcal{R}$ does not affect residence times in a state, and therefore does not change the duration of a trajectory.

We now introduce the quantity

$$A[\gamma] \equiv \ln \frac{P(I)}{P(J)} + \ln \frac{\mathcal{P}[\gamma|I]}{\mathcal{P}[\mathcal{R}\gamma|\widetilde{J}]}. \tag{A5}$$

This quantity bears some resemblance to entropy production, e.g., it satisfies a fluctuation relation $\langle \exp(-A)\rangle = 1$ and is identical to the microscopic entropy production $\Delta s[\gamma]$ if γ does not contain any cycles between I and J because in this case $\mathcal{R}$ coincides with time reversal. We combine Eq. (A5) and Eq. (A2) to write

$$\begin{aligned}P(I)\Psi_{I\to J}(t) &= P(I) \sum_{\gamma|I\overset{t}{\to}J} \mathcal{P}[\gamma|I]\\ &= P(J) \sum_{\gamma|I\overset{t}{\to}J} \mathcal{P}[\mathcal{R}\gamma|\widetilde{J}] e^{A[\gamma]},\end{aligned} \tag{A6}$$

where the notation $I \overset{t}{\to} J$ indicates that summation is over paths γ from I to J of length t. Combining the definition of $\hat{a}_{IJ}(t)$ in (3) with Eqs. (A2) and (A6), we obtain

$$\begin{aligned}e^{\hat{a}_{IJ}(t)} &= \frac{P(I)\Psi_{I\to J}(t)}{P(J)\Psi_{\tilde{J}\to\tilde{I}}(t)} = \frac{\sum_{\gamma|I\overset{t}{\to}J} \mathcal{P}[\mathcal{R}\gamma|\widetilde{J}] e^{A[\gamma]}}{\sum_{\gamma|I\overset{t}{\to}J} \mathcal{P}[\mathcal{R}\gamma|\widetilde{J}]}\\ &= \langle e^{A[\gamma]}\rangle_{\text{aux}},\end{aligned} \tag{A7}$$

and in the last equality identify the expression as a mean with respect to an auxiliary probability measure. Thus, $\inf_{\gamma|I\overset{t}{\to}J} e^{A[\gamma]} \leqslant \langle \exp A[\gamma]\rangle_{\text{aux}} \leqslant \sup_{\gamma|I\overset{t}{\to}J} e^{A[\gamma]}$, which is equivalent to

$$\inf_{\gamma|I\overset{t}{\to}J} A[\gamma] \leqslant \hat{a}_{IJ}(t) \leqslant \sup_{\gamma|I\overset{t}{\to}J} A[\gamma]. \tag{A8}$$

To recast this relation into the form presented in the main text, we now relate the upper and lower bound on $\hat{a}_{IJ}(t)$ to the microscopic entropy production more explicitly. We first note that for the observed transitions $I = k \to l$ and $J = o \to p$ all paths γ are of the form $k \to l \to \cdots \to o \to p$.

In a first step, we assume that γ is a trimmed path, which implies $\mathcal{R}\gamma = \tilde{\gamma}$. In this case, the formal calculation

$$A[\gamma] = \ln \frac{P(I)}{P(J)} + \ln \frac{\mathcal{P}[\gamma|I]}{\mathcal{P}[\mathcal{R}\gamma|\widetilde{J}]} = \ln \frac{p^s_k k_{kl}}{p^s_o k_{op}} + \ln \frac{\mathcal{P}[\gamma|l]}{\mathcal{P}[\mathcal{R}\gamma|o]} \tag{A9}$$

$$= \ln \frac{\mathcal{P}[\gamma,\ \text{excluding } o\to p]}{\mathcal{P}[\widetilde{\gamma},\ \text{excluding } p\to o]} = \Delta s[\gamma] \tag{A10}$$

establishes that A coincides with the physical entropy production excluding the final transition. For a general γ that may include hidden cycles, we replace the second line in the previous calculation with

$$A[\gamma] = \ln \frac{\mathcal{P}[\hat{\gamma},\ \text{excluding } o\to p]}{\mathcal{P}[\widetilde{\hat{\gamma}},\ \text{excluding } p\to o]} = \Delta s[\hat{\gamma}], \tag{A11}$$

which makes use of the fact that $\mathcal{R}$ acts like time reversal on the trimmed path, but does not reverse the direction of cycles, so that their contribution to the path weight in the denominator cancels with a corresponding term in the numerator.

As a consequence of the identification $A[\gamma] = \Delta s[\hat{\gamma}]$, we also see that the upper and lower bound in (A8) are independent of t, because residence times within states contribute to the time-symmetric part of a path weight and therefore do not affect entropy production. Therefore, the same bounds hold true for all t in the inequalities (A8), allowing the reformulation

$$\min_{\gamma|I\to J} \Delta s[\hat{\gamma}] \leqslant \inf_t \hat{a}_{IJ}(t) \leqslant \sup_t \hat{a}_{IJ}(t) \leqslant \max_{\gamma|I\to J} \Delta s[\hat{\gamma}], \tag{A12}$$

which appears as inequality (5). We note that "inf" and "sup" from (A8) have been replaced by "min" and "max," respectively, because there are only finitely many distinct values of $\Delta s[\hat{\gamma}]$ corresponding to the different possible trimmed paths from I to J.

APPENDIX B: GENERAL METHOD TO RECONSTRUCT REALIZATIONS OF A MINIMAL GRAPH

Based on the refined approach to reconstruct a minimal graph illustrated in Sec. VI C, we present an algorithm for arbitrary Markov networks, which differs slightly from the simplified flowchart Fig. 8 in Sec. VI D. For a general network with a set of $N_{1,\dots}$ and $u_{\dots} + N_{1,\dots}$, the following pseudocode describes an algorithm designed to yield the minimal graph if it is unique or all of its putative realizations otherwise.

The Algorithm 1 consists of four logical blocks A through D, in which lines (instructions) are numbered and indentations highlight instructions within loops and conditionals. Additionally, we highlight that the algorithm may generate multiple putative realizations in separate graphs. The remaining steps of the algorithm then need to be applied to these graphs separately.

The first block (A) makes use of the pair rule, which we have discussed in Sec. V, to identify the maximum number N_{Cl} of putative clusters (PCs) and the set $\mathcal{C}$ containing sets of visible links lying in the same of the N_{Cl} PCs. Block B uses these intermediate results to connect one visible link from each PC to one of each neighboring PC. When selecting links

ALGORITHM 1. drawMinimalGraph($N_{1,\dots}$, $u_{\dots}$).

A1: `Determine for all pairs in` $\{I_\pm, J_\pm, K_\pm, \dots\}$ `whether or not they lie in the same putative cluster (PC)`
A2: $N_{\mathrm{Cl}} \widehat{=}$ `max. number of clusters;` $\mathcal{C} = \{\{I_\pm, L_\pm, \dots\}, \{J_\pm, \dots\}, \dots\} \widehat{=}$ `set of sets of visible links lying in the same of the` N_{Cl} `PCs`
B1: $n \coloneqq N_{\mathrm{Cl}}, x \coloneqq 0, y \coloneqq 2$
B2: **Do**
B3: `Select [one of] the pair[s] of` x `drawn and` y `not yet drawn links` $A_\pm, B_\pm$ `with smallest` N_{1,A_aB_b} $(a, b \in \{+,-\})$ `[that lie for` $N_{\mathrm{Cl}} > 1$ `in distinct PCs]`
B4: `Draw the undrawn link(s)` $(A_\pm,)B_\pm$ `and [one of] the shortest path[s] connecting` $A_\pm$ `and` $B_\pm$`. If there are several distinct realizations thereof, generate a separate graph for each of them.`
B5: $n \coloneqq n-1, x \coloneqq 1, y \coloneqq 1$
B6: **while** $n > 1$
C1: **Do**
C2: `Select an unlabeled set from` $\mathcal{C}$`, the PC of which is connected to the largest number of other PCs, and label it` c_n
C3: $f_1(c_n,$ *"shortest"*, *"the same"*$)$
C4: $n \coloneqq n+1$
C5: **while** $n \leqslant N_{\mathrm{Cl}}$
C6: `Delete labels` c_n
C7: $f_2(N_{\mathrm{Cl}}, \mathcal{C},$ *"shortest"*$)$
C8: **If** C7 `returns realizations with updated` N_{Cl} `and` $\mathcal{C}$:
C9: `Discard all realizations with updated` N_{Cl} `and` $\mathcal{C}$`, and restart from line` B1 `for each of the updated combinations` $N_{\mathrm{Cl}}, \mathcal{C}$
C10: **end if**
D1: $n \coloneqq 1$
D2: **Do**
D3: `From` $\mathcal{C}$`, select an unlabeled set, the PC of which is connected to the largest number of other PCs, and label it` c_n
D4: $f_1(c_n,$ *"second-shortest"*, *"the same"*$)$
D5: $n \coloneqq n+1$
D6: **while** $n \leqslant N_{\mathrm{Cl}}$
D7: `Delete labels` c_n
D8: $f_2(N_{\mathrm{Cl}}, \mathcal{C},$ *"second-shortest"*$)$
D9: **If** D8 `returns realizations with updated` N_{Cl} `and` $\mathcal{C}$:
D10: `Discard all realizations with updated` N_{Cl} `and` $\mathcal{C}$`, and restart from line` B1 `for each of the updated combinations` $N_{\mathrm{Cl}}, \mathcal{C}$
D11: **end if**

to draw, there might be sequences of visible links with equal $N_{1,\dots}$. In these cases and all similar cases in later blocks, we arbitrarily choose one of the corresponding paths. For block B, this leads to a tree-like graph, which consists of one visible link of each PC with a shortest path to a visible link of each neighboring PC.

The loop in block C generates realizations with shortest paths between all visible links by consecutively invoking functions f_1 and f_2. These functions both depend on $N_{1,\dots}$ and $u_{\dots}$, which we omit in our notation for the sake of brevity. Function Algorithm 2 generates, with its default arguments "*shortest*" and "*the same*," in all putative realizations all shortest paths within the PC that corresponds to the set $c_n \in \mathcal{C}$ as follows.

For the default arguments, line A4 needs to be executed in a way that may change which links and states form a bridge but keeps neighboring PCs connected by a bridge. Moreover, we stress that putative realizations resulting from this line must respect the relevant $N_{1,L_iI_i\setminus K}$ introduced in Sec. IV for the smallest set K of visible transitions that are considered to be hidden.

Function Algorithm 3 generates, for its default argument "*shortest,*" shortest paths between PCs beginning in the tree of PCs with the outer ones as follows.

For each iteration, line A4 may lead to modified bridges or merged PCs. Thereby, either N_{Cl} and $\mathcal{C}$ remain unchanged for a realization or they change due to merging two or more PCs by drawing a path between two PCs that contains not all of the bridges formerly connecting them. In these latter cases, the function f_2 exits via line E3, whereupon the Algorithm 1 proceeds with deleting the corresponding graph and restarting with the updated quantities in line B1 because finding all putative new realizations is crucial.

Block D is the analogous procedure focusing on second-shortest paths. Thereafter, additional information or methods might allow discarding realizations and extending others with indications of yet undrawn subgraphs. Such methods may be based on specific characteristics of the graph between visible transitions, examples of which we present in Appendix C. In the end, the remaining realizations contain shortest and second-shortest self-avoiding paths. In particular, they are all realizations of the minimal graph that are compatible with the

ALGORITHM 2. $f_1(c_n,$ "*shortest*", "*the same*").

A1: $m \coloneqq 1$
A2: **Do**
A3: `Select (a yet unmarked)` $L_\pm \in c_n$ `with [one of] the` *shortest* `path[s], from` L_l `to` I_i `with` $l, i \in \{+,-\}$`, for an already drawn` $I_\pm$ `in` *the same* `PC (where` $L_\pm = I_\pm$ `due to` $N_{1,I_+I_-} = 0$ `is allowed in the case of "`*the same*`"). Mark` $L_\pm$`.`
A4: `Draw` $L_\pm$ `if it is not yet drawn and the` *shortest* `hidden paths between` $L_\pm$ `and any already drawn visible link in` *the same* `PC. If there are several distinct realizations thereof, generate a separate graph for each of them. [For the case of "`*second-shortest,*`" mind the initial ambiguity of` $u_{L_iI_i} = 1$ `discussed in Sec. IV.]`
A5: `Check each realization for respecting all` $N_{1,\dots}$ `and` $u_{\dots}$ `of drawn links and discard those that do not.`
A6: $m \coloneqq m + 1$
A7: **while** $m \leqslant |c_n|$
A8: `Unmark visible links`
E1: **Result:** `Putative realizations with` *shortest* `paths between all links in` c_n

information used about the given nonequilibrium process. If only one realization results, it is the minimal graph.

Note that this algorithm is designed to provide a supporting structure to find all putative realizations and is not verified to be optimal. As an example, deleting existing realizations for which N_{Cl} and $\mathcal{C}$ have changed is not strictly necessary in lines C9 and D10. Without this, we would then jump to line C1 setting $n = 1$. In this block (C), we would however need to generate putative alternatives for existing paths between visible links, which is less straightforward to describe unambiguously but may speed up the algorithm. Similarly, another route could be adding and completing cycles before drawing paths between distinct visible links. Yet, selecting an approach is like choosing between high road and low road—only at the end do we know which route is faster.

APPENDIX C: ADDITIONAL METHODS FOR GRAPH RECONSTRUCTIONS

1. Cyclic rate product and steady state condition

Rates of visible transitions I as well as of hidden transitions along a path $i \xrightarrow{I} j \to k \xrightarrow{J} l$ with $N_{1,IJ} = 1$ follow from the short-time limit $t \to 0$ as

$$k_{ij} = \lim_{t\to 0} \Psi_{I\to I}(t) \quad \text{and} \tag{C1}$$

$$k_{jk} = \lim_{t\to 0} \Psi_{I\to J}(t)/(t k_{kl}), \tag{C2}$$

respectively, since the product of transition rates of the shortest path between I and J dominates $\Psi_{I\to J}(t)$ in this limit [51]. As shorthand, we define the set $\mathcal{V}_i$ to contain all transitions for which the rates are inferable. These rates allow us to infer additional information about hidden edges near visible ones in specific situations we will discuss now.

First, consider inferred rates k_{jj+1} of a cycle that corresponds to $N_{1,II} = n$. An inequality in

$$\ln\left(\prod_{j=1}^{n} k_{jj+1}\right) \stackrel{?}{=} \lim_{t\to 0} \ln\left(\Psi_{I\to I}(t)\frac{n!}{t^n}\right) \tag{C3}$$

reveals the existence of at least one more cycle with $N_{1,II} = n$.

Hence, this test may provide insight when $u_{IJ} = 1$ so that, as discussed in Sec. IV, a degenerate shortest path is possible. If we are able to determine the transition rates via Eqs. (C1) and (C2), both sides of Eq.(C3) can be determined and compared. If the results do not match, we know for certain that the shortest path is indeed degenerate. We illustrate this point with a network from the main text, namely, the one shown in Fig. 3. We assume that only the number of hidden transitions along shortest paths have been inferred. For the cycle $1 \to 2 \to 3 \to 1$, Eqs. (C1) and (C2) yield all rates k_{jj+1}. Furthermore, comparison (C3) becomes an inequality due to the cycle $1 \to 2 \to 6 \to 1$ containing $R_\pm$ and $N_{1,R_+R_+} = 2$ hidden transitions, and is therefore able to detect this additional cycle.

ALGORITHM 3. $f_2(N_{\mathrm{Cl}}, \mathcal{C},$ "*shortest*").

A1: $m \coloneqq 1$
A2: **Do**
A3: `Select one of the unlabeled PCs with the smallest amount of neighboring PCs in the tree of PCs. Label it` m `and its set in` $\mathcal{C}$ `as` c_m`.`
A4: $f_1(c_m,$ "*shortest*", "*a distinct*")
E1: **If** N_{Cl} `decreases for a putative realization:`
E2: `Update` N_{Cl} `and` $\mathcal{C}$ `only for all of these putative realizations separately`
E3: `Exit this function for these putative realizations`
E4: **end if**
A6: $m \coloneqq m + 1$
A7: **while** $m \leqslant N_{\mathrm{Cl}}$
E5: **Result:** `Putative realizations with` *shortest* `paths`

TABLE III. Transition rates of the multicyclic 10-state network in Fig. 1.

State 1	State 2	State 3	State 4	State 5	State 6	State 7	State 8	State 9	State 10
$k_{12} = 1.0$	$k_{21} = 1.0$	$k_{32} = 1.0$	$k_{42} = 2.5$	$k_{54} = 3.0$	$k_{65} = 1.0$	$k_{74} = 1.0$	$k_{83} = 1.0$	$k_{98} = 1.0$	$k_{101} = 2.0$
$k_{110} = 2.0$	$k_{23} = 1.0$	$k_{34} = 1.0$	$k_{43} = 3.0$	$k_{56} = 1.0$	$k_{67} = 4.0$	$k_{76} = 1.0$	$k_{86} = 8.0$	$k_{910} = 4.0$	$k_{109} = 1.0$
	$k_{24} = 1.0$	$k_{38} = 0.2$	$k_{45} = 3.0$		$k_{68} = 1.0$		$k_{89} = 3.0$		
			$k_{47} = 1.0$						

Second, for a transition $I = (ij)$, its mean observed rate $\langle \dot{n}_I \rangle_{\rm s}$ and the rate k_{ij} determine the steady-state probability $p_i^{\rm s}$ by $p_i^{\rm s} = \langle \dot{n}_I \rangle_{\rm s}/k_{ij}$ [51]. An inequality in

$$\partial_t p_i^{\rm s} = 0 \stackrel{?}{=} \sum_{ij\in\mathcal{V}_i} \left(p_i^{\rm s} k_{ij} - p_j^{\rm s} k_{ji}\right) = \sum_{ij\in\mathcal{V}_i} j_{ij}^{\rm s}, \tag{C4}$$

where we sum over the set $\mathcal{V}_i$ of known, inferable net currents involving state i on the right-hand side, suggests the existence of additional hidden edges that begin/end at state i.

An alternative uses the escape rate

$$\Gamma_i = -\lim_{t\to 0} \frac{\rm d}{{\rm d}t} \ln \frac{\Psi_{\tilde{I}\to I}(t)}{k_{ij}} \tag{C5}$$

of state i, which dominates the exponential decay of $\Psi_{\tilde{I}\to I}(t)$ in the short-time limit. Since this rate equals the sum over all rates of transitions leaving state i, an inequality in

$$\Gamma_i \stackrel{?}{=} \sum_{ij\in\mathcal{V}_i} k_{ij} \tag{C6}$$

again implies at least one additional existing hidden edge at state i. In the example discussed in Sec. VI B, where we reconstruct the graph shown in Fig. 3, finding an inequality in comparison (C4) or (C6) for state 3 would mean that the true graph includes at least one more edge starting at state 3. Such a finding indicates that the minimal graph is not the full one and provides a starting point fur further inference, which can be marked in the minimal graph(s).

2. Entropy production along paths and affinities

For a Markov network in a NESS with only one self-avoiding path between two visible links $I_\pm, J_\pm$, as is the case in, e.g., Fig. 7(a), entropy production along each observed trajectory is constant. Consequently and in analogy to the cycle affinity discussed in Ref. [28], the quantity

$$a_{I_+J_+}(t) = \ln \frac{\Psi_{I_+\to J_+}(t)}{\Psi_{J_-\to I_-}(t)} \tag{C7}$$

is constant and reduces to the logarithmic ratio of rates along the path of $I_+ \to J_+$ and the path of $J_- \to I_-$, which, e.g., yields $a_{L_+R_+}(t) = a_{L_+R_+} = \ln(k_{45}k_{56}k_{67}/k_{65}k_{54}k_{41})$ for the graph shown in Fig. 7(a). Moreover, we have

$$\begin{aligned} a_{L_+R_+}(t) + a_{R_+L_-}(t) &= a_{L_+R_+} + a_{R_+L_-} \\ &= \ln \frac{k_{45}k_{56}k_{67}}{k_{65}k_{54}k_{41}} + \ln \frac{k_{75}k_{54}k_{41}}{k_{45}k_{57}k_{76}} \\ &= \ln \frac{k_{56}k_{67}k_{75}}{k_{65}k_{57}k_{76}} = a_{R_+R_+} = a_{R_+R_+}(t) \end{aligned} \tag{C8}$$

in this example. We note that the quantity (C8) differs from $\hat{a}_{\dots}(t)$ as introduced in the main text in definition (3) only by an additional term $\ln[P(R_-)/P(R_+)]$.

Given a candidate for a minimal graph like the one in Fig. 7(c), such consistency checks provide additional evidence supporting that the minimal graph is correct. In the general situation, explicitly verifying equalities like Eq. (C8) provide a necessary criterion only, because in topologies with degenerate shortest paths relations like (C8) and (C3) are not valid. Under the additional conditions that there are no degenerate shortest paths and no additional self-avoiding paths with the same entropy production, however, consistency checks like (C8) provide another necessary and sufficient criterion to conclude uniqueness of a hidden path between two transitions, in addition to constancy of the quantities $a_{\dots}(t) = \text{const.}$ themselves.

For the graph in Fig. 3 for example, the constant $\hat{a}_{L_+R_-}(t)$ leads to $u_{L_+R_-} = 0$, which means that we do not find an additional path between L_+ and R_- with entropy production differing from the one along the shortest path (cf. Sec. IV). In this example the minimal graph is consistent with both constancy of the $\hat{a}_{\dots}(t)$ in time and the consistency check (C8). As a consequence, the minimal graph has no additional self-avoiding paths between states 2 and 4, which is in agreement with the true graph. In this sense, this consistency check provides a restriction on both the minimal graph and possible extensions.

APPENDIX D: MODEL PARAMETERS AND SIMULATION

1. Multicyclic 10-state network for the illustration of topological inference in Fig. 1

The multicyclic 10-state network in Fig. 1 contains 10 hidden states, 12 hidden links, and 1 visible pair of transitions. The transition rates given in Table III lead to the waiting-time distributions that are shown in Figs. 1(b) and 1(c) and used for the logarithmic ratio $\hat{a}_{++}(t)$ as defined in Eq. (3) and illustrated in Fig. 1(d). The waiting-time distributions can be derived from the solution of initial value problems based on the absorbing network, in which observed transitions are redirected into auxiliary states [28,56].

2. Multicyclic 10-state network for the illustration of entropy production along paths in Fig. 2

The graph of the multicyclic 10-state network in Fig. 2 differs from the graph of the network in Fig. 1 by its visible links $I_\pm$ and $J_\pm$. The transition rates given in Table IV determine the NESS of the network whose entropy production along trajectories from I_+ to J_+ excluding the last transition is shown in Fig. 2(b). The microscopic entropy production along the

TABLE IV. Transition rates of the multicyclic 10-state network used to illustrate coarse-grained and microscopic entropy production along paths in Fig. 2(b).

State 1	State 2	State 3	State 4	State 5	State 6	State 7	State 8	State 9	State 10
$k_{12} = 0.45$	$k_{21} = 0.45$	$k_{32} = 16.59$	$k_{42} = 1.41$	$k_{54} = 1.69$	$k_{65} = 47.53$	$k_{74} = 0.45$	$k_{83} = 0.56$	$k_{98} = 0.45$	$k_{101} = 2.25$
$k_{110} = 2.25$	$k_{23} = 16.59$	$k_{34} = 0.84$	$k_{43} = 1.27$	$k_{56} = 237.66$	$k_{67} = 1.80$	$k_{76} = 0.45$	$k_{86} = 4.50$	$k_{910} = 1.80$	$k_{109} = 0.45$
	$k_{24} = 0.56$	$k_{38} = 0.11$	$k_{45} = 1.69$		$k_{68} = 0.56$		$k_{89} = 1.35$		
			$k_{47} = 0.45$						

three paths from I_+ to J_+ directly results from the transition rates of their forward and backward direction. The coarse-grained entropy production can be derived from the rates, the stationary state and the waiting-time distributions, which are determined as described in the previous Appendix D 1.

For the 1 731 699 networks for which the scatter plot in Fig. 2(c) displays the ratio of differences between microscopic and between coarse-grained entropy productions along trajectories from I_+ to J_+, we have randomly drawn all transition rates listed in Table IV from the uniform distribution $\Theta(0.5, 10)$ that is defined between 0.5 and 10. The binned mean of the shown data has been determined in bins of width 0.1 for $\Delta s[\gamma_1] \in [-4, 4)$, in bins of width 1.0 for $-6 \leqslant \Delta s[\gamma_1] < 4$ and $4 \leqslant \Delta s[\gamma_1] < 6$, and in one bin for other values of $\Delta s[\gamma_1]$ on either side of zero.

[1] K. Sekimoto, *Stochastic Energetics* (Springer, Berlin, 2010).

[2] C. Jarzynski, Equalities and inequalities: Irreversibility and the second law of thermodynamics at the nanoscale, Annu. Rev. Condens. Matter Phys. **2**, 329 (2011).

[3] U. Seifert, Stochastic thermodynamics, fluctuation theorems, and molecular machines, Rep. Prog. Phys. **75**, 126001 (2012).

[4] L. Peliti and S. Pigolotti, *Stochastic Thermodynamics. An Introduction* (Princeton University Press, Princeton, 2021).

[5] N. Shiraishi, *An Introduction to Stochastic Thermodynamics*, Fundamental Theories of Physics (Springer Nature Singapore, Singapore, 2023).

[6] U. Seifert, From stochastic thermodynamics to thermodynamic inference, Annu. Rev. Condens. Matter Phys. **10**, 171 (2019).

[7] A. C. Barato and U. Seifert, Thermodynamic uncertainty relation for biomolecular processes, Phys. Rev. Lett. **114**, 158101 (2015).

[8] T. R. Gingrich, J. M. Horowitz, N. Perunov, and J. L. England, Dissipation bounds all steady-state current fluctuations, Phys. Rev. Lett. **116**, 120601 (2016).

[9] J. M. Horowitz and T. R. Gingrich, Thermodynamic uncertainty relations constrain non-equilibrium fluctuations, Nat. Phys. **16**, 15 (2020).

[10] N. Shiraishi, K. Funo, and K. Saito, Speed limit for classical stochastic processes, Phys. Rev. Lett. **121**, 070601 (2018).

[11] S. Ito and A. Dechant, Stochastic time evolution, information geometry, and the Cramér-Rao bound, Phys. Rev. X **10**, 021056 (2020).

[12] A. Dechant, Minimum entropy production, detailed balance and Wasserstein distance for continuous-time Markov processes, J. Phys. A: Math. Theor. **55**, 094001 (2022).

[13] T. Van Vu and K. Saito, Thermodynamic unification of optimal transport: Thermodynamic uncertainty relation, minimum dissipation, and thermodynamic speed limits, Phys. Rev. X **13**, 011013 (2023).

[14] R. Nagayama, K. Yoshimura, and S. Ito, Infinite variety of thermodynamic speed limits with general activities, Phys. Rev. Res. **7**, 013307 (2025).

[15] A. Dechant and S.-i. Sasa, Fluctuation—Response inequality out of equilibrium, Proc. Natl. Acad. Sci. USA **117**, 6430 (2020).

[16] J. A. Owen, T. R. Gingrich, and J. M. Horowitz, Universal thermodynamic bounds on nonequilibrium response with biochemical applications, Phys. Rev. X **10**, 011066 (2020).

[17] T. Aslyamov and M. Esposito, Nonequilibrium response for Markov jump processes: Exact results and tight bounds, Phys. Rev. Lett. **132**, 037101 (2024).

[18] N. Ohga, S. Ito, and A. Kolchinsky, Thermodynamic bound on the asymmetry of cross-correlations, Phys. Rev. Lett. **131**, 077101 (2023).

[19] N. Shiraishi, Entropy production limits all fluctuation oscillations, Phys. Rev. E **108**, L042103 (2023).

[20] D. J. Skinner and J. Dunkel, Estimating entropy production from waiting time distributions, Phys. Rev. Lett. **127**, 198101 (2021).

[21] A. Dechant, J. Garnier-Brun, and S.-i. Sasa, Thermodynamic bounds on correlation times, Phys. Rev. Lett. **131**, 167101 (2023).

[22] P. Pietzonka and F. Coghi, Thermodynamic cost for precision of general counting observables, Phys. Rev. E **109**, 064128 (2024).

[23] M. Esposito, Stochastic thermodynamics under coarse graining, Phys. Rev. E **85**, 041125 (2012).

[24] S. Bo and A. Celani, Multiple-scale stochastic processes: Decimation, averaging and beyond, Phys. Rep. **670**, 1 (2017).

[25] N. Shiraishi and T. Sagawa, Fluctuation theorem for partially masked nonequilibrium dynamics, Phys. Rev. E **91**, 012130 (2015).

[26] M. Polettini and M. Esposito, Effective fluctuation and response theory, J. Stat. Phys. **176**, 94 (2019).

[27] I. A. Martínez, G. Bisker, J. M. Horowitz, and J. M. R. Parrondo, Inferring broken detailed balance in the absence of observable currents, Nat. Commun. **10**, 3542 (2019).

[28] J. van der Meer, B. Ertel, and U. Seifert, Thermodynamic inference in partially accessible markov networks: A unifying perspective from transition-based waiting time distributions, Phys. Rev. X **12**, 031025 (2022).

[29] P. Harunari, A. Dutta, M. Polettini, and E. Roldan, What to learn from a few visible transitions' statistics? Phys. Rev. X **12**, 041026 (2022).

[30] A. Gomez-Marin, J. M. R. Parrondo, and C. Van den Broeck, Lower bounds on dissipation upon coarse-graining, Phys. Rev. E **78**, 011107 (2008).

[31] E. Roldan and J. M. R. Parrondo, Estimating dissipation from single stationary trajectories, Phys. Rev. Lett. **105**, 150607 (2010).

[32] S. Muy, A. Kundu, and D. Lacoste, Non-invasive estimation of dissipation from non-equilibrium fluctuations in chemical reactions, J. Chem. Phys. **139**, 124109 (2013).

[33] P. E. Harunari, A. Garilli, and M. Polettini, Beat of a current, Phys. Rev. E **107**, L042105 (2023).

[34] J. Degünther, J. van der Meer, and U. Seifert, Fluctuating entropy production on the coarse-grained level: Inference and localization of irreversibility, Phys. Rev. Res. **6**, 023175 (2024).

[35] J. Degünther, J. van der Meer, and U. Seifert, General theory for localizing the where and when of entropy production meets single-molecule experiments, Proc. Natl. Acad. Sci. USA **121**, e2405371121 (2024).

[36] D. Hartich and A. Godec, Emergent memory and kinetic hysteresis in strongly driven networks, Phys. Rev. X **11**, 041047 (2021).

[37] K. Blom, K. Song, E. Vouga, A. Godec, and D. E. Makarov, Milestoning estimators of dissipation in systems observed at a coarse resolution, Proc. Natl. Acad. Sci. USA **121**, e2318333121 (2024).

[38] J. van der Meer, J. Degünther, and U. Seifert, Time-resolved statistics of snippets as general framework for model-free entropy estimators, Phys. Rev. Lett. **130**, 257101 (2023).

[39] O. A. Igoshin, A. B. Kolomeisky, and D. E. Makarov, Coarse-graining chemical networks by trimming to preserve energy dissipation, J. Phys. Chem. Lett. **16**, 1229 (2025).

[40] X. Li and A. B. Kolomeisky, Mechanisms and topology determination of complex chemical and biological network systems from first-passage theoretical approach, J. Chem. Phys. **139**, 144106 (2013).

[41] A. M. Berezhkovskii, G. Hummer, and S. M. Bezrukov, Identity of distributions of direct uphill and downhill translocation times for particles traversing membrane channels, Phys. Rev. Lett. **97**, 020601 (2006).

[42] A. M. Berezhkovskii and D. E. Makarov, On the forward/backward symmetry of transition path time distributions in nonequilibrium systems, J. Chem. Phys. **151**, 065102 (2019).

[43] J. Gladrow, M. Ribezzi-Crivellari, F. Ritort, and U. F. Keyser, Experimental evidence of symmetry breaking of transition-path times, Nat. Commun. **10**, 55 (2019).

[44] G. R. Bowman, V. S. Pande, and F. Noé, editors, *An Introduction to Markov State Models and Their Application to Long Timescale Molecular Simulation* (Springer, Dordrecht, 2014).

[45] L. Vollmar, J. Schimpf, B. Hermann, and T. Hugel, Cochaperones convey the energy of ATP hydrolysis for directional action of Hsp90, Nat. Commun. **15**, 569 (2024).

[46] L. Vollmar, R. Bebon, J. Schimpf, B. Flietel, S. Celiksoy, C. Sönnichsen, A. Godec, and T. Hugel, Model-free inference of memory in conformational dynamics of a multi-domain protein, J. Phys. A: Math. Theor. **57**, 365001 (2024).

[47] I. Neri and M. Polettini, Extreme value statistics of edge currents in Markov jump processes and their use for entropy production estimation, SciPost Phys. **14**, 131 (2023).

[48] F. Jülicher, A. Ajdari, and J. Prost, Modeling molecular motors, Rev. Mod. Phys. **69**, 1269 (1997).

[49] P. Gaspard and E. Gerritsma, The stochastic chemomechanics of the F_1-ATPase molecular motor, J. Theor. Biol. **247**, 672 (2007).

[50] E. Zimmermann and U. Seifert, Efficiency of a molecular motor: A generic hybrid model applied to the F_1-ATPase, New J. Phys. **14**, 103023 (2012).

[51] A. M. Maier, J. Degünther, J. van der Meer, and U. Seifert, Inferring kinetics and entropy production from observable transitions in partially accessible, periodically driven markov networks, J. Stat. Phys. **191**, 104 (2024).

[52] P. E. Harunari, C. E. Fiore, and A. C. Barato, Inference of entropy production for periodically driven systems, Phys. Rev. E **110**, 064126 (2024).

[53] A. Godec and D. E. Makarov, Challenges in inferring the directionality of active molecular processes from single-molecule fluorescence resonance energy transfer trajectories, J. Phys. Chem. Lett. **14**, 49 (2023).

[54] O. A. Igoshin, A. B. Kolomeisky, and D. E. Makarov, Uncovering dissipation from coarse observables: A case study of a random walk with unobserved internal states, J. Chem. Phys. **162**, 034111 (2025).

[55] X. Li, A. B. Kolomeisky, and A. Valleriani, Pathway structure determination in complex stochastic networks with non-exponential dwell times, J. Chem. Phys. **140**, 184102 (2014).

[56] K. Sekimoto, Derivation of the first passage time distribution for Markovian process on discrete network, arXiv:2110.02216.